

# Direct tau production at hadron colliders in cosmologically motivated scenarios

---

**Jonas M. Lindert, Frank D. Steffen**

*Max-Planck-Institut für Physik, Föhringer Ring 6, D-80805 München, Germany*

*Email: lindert@mpp.mpg.de, steffen@mpp.mpg.de*

**Maike K. Trenkel**

*Phenomenology Institute, Department of Physics, University of Wisconsin-Madison,  
1150 University Avenue, Madison, Wisconsin 53706, USA*

*Email: trenkel@hep.wisc.edu*

**ABSTRACT:** We calculate dominant cross section contributions for tau pair production at hadron colliders within the MSSM, taking into account left-right mixing of the tau eigenstates. We find that  $b$ -quark annihilation and gluon fusion can enhance the cross sections by more than one order of magnitude with respect to the Drell–Yan predictions. These additional production channels are not yet included in the common Monte Carlo analysis programs and have been neglected in experimental analyses so far. For long-lived taus, we investigate differential distributions and prospects for their stopping in the collider detectors. New possible strategies are outlined to determine the mass and width of the heavy CP-even Higgs boson  $H^0$ . Scans of the relevant regions in the CMSSM are performed and predictions are given for the current experiments at the LHC and the Tevatron. The obtained insights allow us to propose collider tests of cosmologically motivated scenarios with long-lived taus that have an exceptionally small thermal relic abundance.

**KEYWORDS:** Supersymmetry Phenomenology, Hadronic Colliders, Cosmology of Theories Beyond the Standard Model.

---

## Contents

<b>1. Introduction</b>	<b>1</b>
<b>2. Motivation</b>	<b>4</b>
2.1 Gravitino/axino dark matter scenarios with a long-lived stau NLSP	5
2.2 Thermal relic abundances of long-lived staus and cosmological constraints	6
2.3 Exceptionally small thermal relic stau abundances	7
<b>3. Direct production of stau pairs at hadron colliders</b>	<b>9</b>
3.1 Direct $\tilde{\tau}_1 \tilde{\tau}_1^*$ production channels	10
3.2 Numerical results	12
<b>4. Collider phenomenology with directly produced long-lived staus</b>	<b>15</b>
4.1 Kinematical cuts	16
4.2 Prospects for SUSY parameter determination	19
4.3 Prospects for the stopping of staus	23
<b>5. Direct stau production within the CMSSM</b>	<b>24</b>
5.1 CMSSM scans of the direct stau pair production cross section	24
5.2 Direct stau production vs. staus from cascade decays	28
<b>6. Collider tests of an exceptionally small relic stau abundance</b>	<b>30</b>
<b>7. Conclusions</b>	<b>37</b>
<b>A. Stau sector in the MSSM</b>	<b>39</b>
A.1 Stau mixing and mass eigenstates	39
A.2 Stau-Higgs couplings	40
<b>B. Resummation in the bottom sector</b>	<b>41</b>

---

## 1. Introduction

The ongoing experiments at the Large Hadron Collider (LHC) allow us to enter new terrain at the TeV scale and to search for new physics in an unprecedented way. In fact, due to the remarkable properties of supersymmetric (SUSY) extensions of the Standard Model (SM) [1–6], there are high hopes to discover superpartners of the SM fields in the mass range probed by the LHC experiments. Such a discovery would be a major breakthrough with far reaching consequences also for our understanding of cosmology and the early

Universe. With the lightest SUSY particle (LSP) being a promising dark matter (DM) candidate [7–9], collider studies may help us to clarify the origin and identity of DM and to probe the early thermal history even prior to primordial nucleosynthesis.

In this work we study the direct pair production of the lighter stau  $\tilde{\tau}_1$  at hadron colliders. The  $\tilde{\tau}_1$  is the lighter one of the two scalar partners of the tau lepton  $\tau$  and often the lightest slepton within the minimal SUSY extension of the SM (MSSM). Among the potential SUSY discovery channels, the production of color-charged SUSY particles, squarks and gluinos, is typically assumed to play a key role since they can be produced via the strong interaction; *cf.* [4–6] and references therein. However, recent searches for signals with jets and missing energy at the LHC [10, 11] disfavor very light squarks and gluinos. In case these searches keep on in setting new limits in the near future, the viable mass range for squarks and gluinos will soon be pushed towards and above 1 TeV [12], where the associated production cross sections drop sharply, especially during the early run of the LHC with a center-of-mass energy of  $\sqrt{S} = 7$  TeV. However, color-singlet SUSY particles such as sleptons, neutralinos, and charginos could still be light enough to be produced in large numbers at colliders. Direct stau production could thereby allow for SUSY discoveries in the near future. On the other hand, non-observation of the direct production channels will allow us to infer exclusion limits on subsets of the SUSY parameter space, independent of the colored sector.

The lighter stau can play a crucial role not only for collider phenomenology but also in cosmology. While the  $\tilde{\tau}_1$  with its electric charge cannot be DM, it can be the next-to-lightest SUSY particle (NLSP) in an R-parity conserving realization of SUSY. If the lightest neutralino  $\tilde{\chi}_1^0$  is the LSP, a stau NLSP that is almost as light as the  $\tilde{\chi}_1^0$  can participate via coannihilation in the primordial freeze-out of the  $\tilde{\chi}_1^0$ . In fact, such a coannihilation scenario might be the key for an agreement of the relic  $\tilde{\chi}_1^0$  density  $\Omega_{\tilde{\chi}_1^0}$  with the DM density  $\Omega_{\text{DM}}$ ; *cf.* [5–9, 13] and references therein. The direct pair production of such light  $\tilde{\tau}_1$ ’s can then have a sizeable cross section at hadron colliders even if the colored sparticles are substantially more massive. Since each of those  $\tilde{\tau}_1$ ’s will decay rapidly into a  $\tilde{\chi}_1^0$ , an excess in missing transverse energy is the expected signature of such a scenario.

There are other well-motivated scenarios in which the lighter stau  $\tilde{\tau}_1$  is central for both cosmology and phenomenology. In fact, in large parts of the parameter space of many constrained SUSY models, such as the constrained MSSM (CMSSM), the lighter stau  $\tilde{\tau}_1$  is the lightest SUSY particle in the MSSM spectrum, to which we refer as the lightest ordinary SUSY particle (LOSP). While restrictive upper limits exist on the abundance of a stable charged massive particle (CHAMP) [14], the  $\tilde{\tau}_1$  LOSP becomes a viable possibility in scenarios with broken R-parity [15–19] or in R-parity-conserving scenarios in which the LSP is an extremely weakly interacting particle (EWIP), such as the gravitino [20–26] or the axino [27–29]. The  $\tilde{\tau}_1$  LOSP can then be long-lived and as such appear in the collider detectors as a quasi-stable muon-like particle. Such scenarios will come with distinctive signatures that are very different from those in the  $\tilde{\chi}_1^0$  LSP case [26, 30–39]. In fact, direct  $\tilde{\tau}_1$ -pair production events will be easier to identify experimentally if the  $\tilde{\tau}_1$  is quasi-stable. It may even be possible to stop initially slow staus within the main detectors [29, 40–42] or in some additional dedicated stopping detectors [30, 43–45] for analyses of their late decays.

The cosmological implications of a long-lived  $\tilde{\tau}_1$  depend on its lifetime  $\tau_{\tilde{\tau}_1}$ , its mass  $m_{\tilde{\tau}_1}$ , and its primordial relic abundance prior to decay  $Y_{\tilde{\tau}_1} \equiv n_{\tilde{\tau}_1}/s$ , where  $n_{\tilde{\tau}_1}$  is its comoving number density prior to decay and  $s$  the entropy density. For example, in the R-parity conserving case with an EWIP LSP, each  $\tilde{\tau}_1$  NLSP decays into one LSP which contributes to the DM density  $\Omega_{\text{DM}}$ . Moreover,  $\tau_{\tilde{\tau}_1}$  can exceed 1–100 s in scenarios with the gravitino LSP [24] or the axino LSP [27–29]. Long-lived  $\tilde{\tau}_1$ ’s can then decay during or after big bang nucleosynthesis (BBN) and the emitted SM particles can reprocess the primordial abundances of deuterium, helium, and lithium [46–49]. Negatively charged  $\tilde{\tau}_1$ ’s may even form bound states with the primordial nuclei leading to catalyzed BBN (CBBN) of lithium-6 and beryllium-9 [50–55]. The DM abundance and the observationally inferred primordial abundances of the light elements thereby impose  $\tau_{\tilde{\tau}_1}$ -dependent upper limits on the yield  $Y_{\tilde{\tau}_1}$  which translate into cosmological constraints on the parameter space of the respective SUSY models; *cf.* [29, 49, 51, 53, 55–61] and references therein.

The cosmological constraints on scenarios with long-lived staus  $\tilde{\tau}_\varphi$  are often quite restrictive with potentially severe implications for collider phenomenology and cosmology. For example, the CBBN constraints on gravitino LSP scenarios can point to heavy colored sparticles, such as a gluino with mass  $m_{\tilde{g}} \gtrsim 2.5$  TeV [51, 53, 57, 59], so that direct stau production would be particularly important for SUSY discoveries at the LHC. Moreover, together with  $\Omega_{\text{DM}}$  limiting the thermally produced EWIP density [57, 62–67] from above, the CBBN constraints can restrict the post-inflationary reheating temperature to  $T_{\text{R}} \ll 10^9$  GeV [57, 61], which disfavors the viability of thermal leptogenesis with hierarchical heavy Majorana neutrino masses [68–72]. In light of those findings, it is remarkable that parameter regions exist in which one finds an exceptionally small relic  $\tilde{\tau}_1$  abundance [73, 74] which may respect the (C)BBN limits on  $Y_{\tilde{\tau}_1}$  so that the above restrictions do no longer apply. Such exceptional yields can result from efficient primordial annihilation of staus with  $m_{\tilde{\tau}_1} \lesssim 200$  GeV via enhanced stau-Higgs couplings [73, 74] and/or stau annihilation at the resonance of the CP-even heavy Higgs boson  $H^0$  [74]. Here in this paper we address the question whether such a scenario with efficient primordial stau annihilation can be identified by considering direct  $\tilde{\tau}_1$ -pair production at hadron colliders.

Our paper provides predictions for direct  $\tilde{\tau}_1$ -pair production cross sections and kinematical distributions at hadron colliders in the framework of the R-parity conserving MSSM. Our calculations include Drell–Yan processes as well as  $b$ -quark annihilation and gluon fusion, where diagrams with s-channel  $h^0$  or  $H^0$  exchange can become dominant. All third generation mixing effects are taken into account. While the obtained cross sections are independent of the stau lifetime, we interpret our findings with a special focus on scenarios with long-lived staus. For such scenarios, we address collider prospects for the SUSY parameter determination, the stopping of slow staus in the detectors, and viability tests of exceptionally small relic stau abundances.

Theoretical predictions for slepton-pair production via the Drell–Yan channel are well known since many years and include next-to-leading order (NLO) corrections from QCD and SUSY-QCD [75–77] and resummation improved results at the next-to-leading logarithmic (NLL) level [78–80]. The NLO QCD and SUSY-QCD results are available via the software package **Prospino** 2 [81]. Also contributions from  $b\bar{b}$  annihilation and from gluon

fusion were studied in refs. [82–84] which focussed on the limit of no left-right mixing. While this limit is usually a good approximation for first and second generation sleptons, the mixing between the (third generation) stau gauge eigenstates can be substantial. Moreover, the  $b\bar{b}$  and  $gg$  channels are not included in the stau-pair production cross section predictions provided by Monte Carlo simulation codes such as *Pythia* [85] or *Herwig* [86]. This provides additional motivation for our present study which considers for the first time all three of the mentioned direct stau production mechanisms with particular emphasis on potentially sizeable left-right mixing.

The outline of this paper is as follows. In the next section we elaborate on the motivation for exploring direct stau production and the considered parameter regions. Section 3 presents our calculation of direct stau production at hadron colliders. Here we show our cross section results for the Tevatron and the LHC and compare the Drell–Yan contributions to those from  $b\bar{b}$ -annihilation and gluon fusion. Section 4 concentrates on scenarios with long-lived staus and associated prospects for the SUSY parameter determination and the stopping of staus. In section 5 we consider the CMSSM for parameters for which exceptionally small  $Y_{\tilde{\tau}_1}$  occur. Here we study representative CMSSM benchmark scenarios also to explore the relative importance of direct stau production with respect to the stau production in cascade decays. In section 6 we explore ways to probe the viability of an exceptionally small relic stau abundance at colliders. As exemplary models we consider the CMSSM and a model with non-universal Higgs masses (NUHM) to illustrate our main points. We summarize our findings in section 7.

## 2. Motivation

In this section we continue to review the various implications of a stau NLSP in collider phenomenology and cosmology. Focussing on gravitino and axino dark matter scenarios with long-lived staus, we address the appearance of such staus in the detectors, existing limits, and the conceivable stopping of staus for studies of their late decays. We describe the typical primordial stau LOSP freeze-out and associated cosmological constraints. Considering the CMSSM with the gravitino LSP, the constraints can point to heavy colored sparticles and one may have to rely on direct stau production for a SUSY discovery at the LHC.

We discuss the possibility of particularly efficient primordial stau annihilation leading to an exceptionally small thermal relic stau abundance such that restrictive cosmological constraints can be evaded. We summarize the conditions required for such a behavior and emphasize that the potential occurrence of a (color and) charge breaking (CCB) vacuum, B-physics observables, and Higgs searches can give restrictions in the relevant parameter regions.

Before proceeding let us comment briefly on direct stau production events in the neutralino dark matter case. As already mentioned in the introduction, the  $\tilde{\tau}_1$  NLSP is an attractive possibility in the  $\tilde{\chi}_1^0$  LSP case and primordial  $\tilde{\chi}_1^0$ – $\tilde{\tau}_1$ -coannihilation processes may even turn out to be crucial for  $\Omega_{\tilde{\chi}_1^0} \simeq \Omega_{\text{DM}}$ . In an R-parity conserving realization of SUSY, we expect each directly produced  $\tilde{\tau}_1 \tilde{\tau}_1^*$  pair to decay into a pair of unlike-sign  $\tau$  leptons

and a  $\tilde{\chi}_1^0$  pair. The emitted  $\tau^+\tau^-$  pair would then help to identify direct  $\tilde{\tau}_1\tilde{\tau}_1^*$  production events experimentally. This identification however requires sophisticated studies since the  $\tilde{\chi}_1^0$ 's and the neutrinos from the rapidly decaying  $\tau$ 's will lead to missing transverse energy. Leaving such studies for further work, we focus in the following more on scenarios with a long-lived  $\tilde{\tau}_1$  LOSP. Nevertheless, our calculations of direct  $\tilde{\tau}_1\tilde{\tau}_1^*$  production cross sections (see section 3) apply also to  $\tilde{\chi}_1^0$  dark matter scenarios with the  $\tilde{\tau}_1$  NLSP.

## 2.1 Gravitino/axino dark matter scenarios with a long-lived stau NLSP

Long-lived staus occur naturally in SUSY extensions of the SM in which the LSP is an EWIP such as the gravitino or the axino. Both of those EWIPs are viable DM candidates which can be produced thermally in the hot primordial plasma with the right relic density,  $\Omega_{\text{EWIP}} \simeq \Omega_{\text{DM}}$ , depending on the reheating temperature  $T_R$  after inflation [57, 62–67]. Both are not part of the MSSM (and thus cannot be the LOSP) but are still very well-motivated:<sup>1</sup>

- The gravitino  $\tilde{G}$  is the gauge field of local SUSY transformations and an unavoidable implication of SUSY theories including gravity [1, 2]. In the course of SUSY breaking, it acquires a mass  $m_{\tilde{G}}$  that can naturally be smaller than the one of the  $\tilde{\tau}_1$  LOSP, for example, in gauge-mediated and gravity-mediated SUSY breaking scenarios [4–6]. The stau lifetime  $\tau_{\tilde{\tau}_1}$  is then governed by the two-body decay  $\tilde{\tau}_1 \rightarrow \tau\tilde{G}$  which involves a supergravity vertex and thereby the Planck scale  $M_{\text{Pl}} = 2.4 \times 10^{18}$  GeV [24]. Moreover,  $\tau_{\tilde{\tau}_1}$  depends sensitively on  $m_{\tilde{G}}$  and  $m_{\tilde{\tau}_1}$  and can easily exceed 100 s, *e.g.*, for  $m_{\tilde{G}} \sim 1$  GeV and  $m_{\tilde{\tau}_1} \lesssim 300$  GeV; *cf.* eq. (4.1) and figure 6 in ref. [55].
- The axino  $\tilde{a}$  is the fermionic superpartner of the axion and appears once the MSSM is extended by the Peccei–Quinn (PQ) mechanism in order to solve the strong CP problem. Its mass  $m_{\tilde{a}}$  is model dependent and can be smaller than  $m_{\tilde{\tau}_1}$ . It is then the two-body decay  $\tilde{\tau}_1 \rightarrow \tau\tilde{a}$  which governs  $\tau_{\tilde{\tau}_1}$  such that it depends on the axion model, the Peccei–Quinn scale  $f_{\text{PQ}} \gtrsim 6 \times 10^8$  GeV [14, 90],  $m_{\tilde{a}}$ , and  $m_{\tilde{\tau}_1}$  [27–29, 61]. Again  $\tau_{\tilde{\tau}_1} \gtrsim 100$  s is possible, *e.g.*, for  $f_{\text{PQ}} \sim 10^{12}$  GeV and  $m_{\tilde{\tau}_1} \lesssim 300$  GeV; *cf.* eq. (22) and figure 3 in ref. [61].

In such settings, a directly produced stau will usually appear as a stable particle in the detector. In fact, already a  $\tilde{\tau}_1$  LOSP lifetime as short as  $\tau_{\tilde{\tau}_1} \approx 10^{-6}$  s is associated with a decay length of  $c\tau_{\tilde{\tau}_1} \approx 300$  m for which typically only a small fraction of the produced staus will decay within the collider detectors. Such quasi-stable staus will look like heavy muons with distinctive signatures in the collider detectors [20–22, 91–94] (see section 4).

Direct searches for long-lived staus at the Large Electron Positron (LEP) collider at CERN set currently the following model-independent limit [14, 95]:<sup>2</sup>

$$m_{\tilde{\tau}_1} \gtrsim 82 \text{ GeV} . \quad (2.1)$$

---

<sup>1</sup>For simplicity, we discuss scenarios in which only the gravitino or only the axino is lighter than the stau. There is also the possibility that the gravitino and axino are both simultaneously lighter than the stau, and we refer to refs. [29, 87–89] for studies of the cosmological and phenomenological implications.

<sup>2</sup>Note that (2.1) is a conservative limit. Also the LEP limit  $m_{\tilde{\tau}_1} \gtrsim 97.5$  GeV can be found [14, 95].

Moreover, searches for long-lived staus in proton-antiproton collisions with  $\sqrt{S} = 1.96$  TeV at the Tevatron [96, 97] have led to the following upper limit on the stau production cross section [97]:

$$\sigma(\sqrt{S} = 1.96 \text{ TeV}) \lesssim 10 \text{ fb} , \quad (2.2)$$

with which we will compare our cross section results in sections 4.1 and 5.

### Stopping of long-lived staus and studies of their late decays

Quasi-stable staus may allow for other intriguing non-standard collider phenomenology. Because of ionisation energy loss, staus will be slowed down when traversing the detector material. In this way, staus that are produced with a relatively small initial velocity of

$$p_{\tilde{\tau}_1}/m_{\tilde{\tau}_1} = \beta\gamma \lesssim 0.45 \quad (2.3)$$

are expected to get trapped, *e.g.*, in the calorimeters of the ATLAS detector [41] or in some additional dedicated stopping detector outside of the CMS detector [45]. This can allow for experimental studies of the stau decays. Measurements of  $\tau_{\tilde{\tau}_1}$  could then probe the coupling strength that governs the stau decays and thereby  $m_{\tilde{G}}$  [24] or the Peccei–Quinn scale  $f_{\text{PQ}}$  [28, 29]. Moreover, one may be able to determine the mass of the EWIP LSP by analyzing the kinematics of the mentioned two-body decays [24, 28, 29, 40, 45]. In the gravitino LSP case, a kinematically determined  $m_{\tilde{G}}$  would allow us to test the Planck scale  $M_{\text{Pl}}$  microscopically [24] and to probe the reheating temperature  $T_{\text{R}}$  at colliders and thereby the viability of thermal leptogenesis [64]. Also studies of three-body stau decays are conceivable, which could give further insights into the nature of the EWIP LSP [24, 28, 29, 45]. The success of such studies will depend sensitively on the number of staus that can be stopped for the analysis of their decays and thereby on the initial velocity distribution. This motivates us to consider such distributions in section 4.3 below.

## 2.2 Thermal relic abundances of long-lived staus and cosmological constraints

Let us now turn to long-lived staus in the early Universe, the potential cosmological implications and associated constraints. The relic stau abundance  $Y_{\tilde{\tau}_1}$  prior to decay depends on  $m_{\tilde{\tau}_1}$ , the left-right mixing of the  $\tilde{\tau}_1$  and other details of the SUSY model, and on the early thermal history of the Universe. For a standard thermal history with a reheating temperature  $T_{\text{R}}$  that exceeds  $m_{\tilde{\tau}_1}/20$ , there was a period in which the  $\tilde{\tau}_1$  LSP was in thermal equilibrium with the primordial plasma. At the freeze-out temperature  $T_{\text{f}} \lesssim m_{\tilde{\tau}_1}/20$ , at which the  $\tilde{\tau}_1$  annihilation rate equals the Hubble rate, the by then non-relativistic staus  $\tilde{\tau}_1$ 's decouple from the thermal plasma. Taking into account all possible (co-)annihilation channels, the associated Boltzmann equation can be solved numerically [98, 99]. For a dominantly right-handed stau,  $\tilde{\tau}_1 \simeq \tilde{\tau}_{\text{R}}$ , the resulting yield is found to be governed mainly by  $m_{\tilde{\tau}_1}$ ,

$$Y_{\tilde{\tau}_1} \simeq (0.4 - 2.0) \times 10^{-13} \left( \frac{m_{\tilde{\tau}_1}}{100 \text{ GeV}} \right) , \quad (2.4)$$

where larger values of the prefactor account for possible mass degeneracies and associated effects such as stau-slepton or stau-neutralino coannihilation [57, 100–102].

Confronting the yield (2.4) with the CBBN constraints (shown *e.g.* in figure 5 of ref. [55]), the following upper limit on the stau lifetime emerges [50, 55]

$$\tau_{\tilde{\tau}_1} \lesssim 5 \times 10^3 \text{ s} . \quad (2.5)$$

For the cases with the gravitino LSP and the axino LSP, this implies  $m_{\tilde{\tau}_1}$ -dependent upper limits on the gravitino mass  $m_{\tilde{G}}$  (*cf.* figure 6 in ref. [55]) and the PQ scale  $f_a$  (*cf.* figure 5 in ref. [103]), respectively. In particular, a PQ scale  $f_{\text{PQ}}$  around the scale of grand unification  $M_{\text{GUT}} \simeq 2 \times 10^{16} \text{ GeV}$  is in conflict with the CBBN constraint for the  $m_{\tilde{\tau}_1}$  range accessible at the LHC [103]. Moreover, the  $m_{\tilde{G}}$  limit disfavors the kinematical  $m_{\tilde{G}}$  determination [56] and thereby both the mentioned  $M_{\text{Pl}}$  determination [24] and the probing of  $T_{\text{R}}$  at colliders [64]. These CBBN limits on  $m_{\tilde{G}}$  and  $f_{\text{PQ}}$  tighten also the upper limits on the reheating temperature  $T_{\text{R}}$  imposed by  $\Omega_{\text{EWIP}} \leq \Omega_{\text{DM}}$  [57, 61]. The resulting  $T_{\text{R}}$  limits can then be in considerable tension with  $T_{\text{R}} \gtrsim 10^9 \text{ GeV}$  required for viable thermal leptogenesis with hierarchical heavy Majorana neutrino masses [68–72].

For CMSSM scenarios with the gravitino LSP, the CBBN constraints have been found to be particularly restrictive [51, 53, 57–59]. In the framework of the CMSSM, the gaugino masses, the scalar masses, and the trilinear scalar interactions are assumed to take on the respective universal values  $m_{1/2}$ ,  $m_0$ , and  $A_0$  at  $M_{\text{GUT}}$ . Specifying those values in addition to the mixing angle in the Higgs sector  $\tan \beta$  and the sign of the Higgs-higgsino-mass parameter  $\mu$ , the low energy mass spectrum is given by the renormalization group running from  $M_{\text{GUT}}$  downwards. Here the  $\tilde{\tau}_1$  LOSP case occurs in a large part of the parameter space and in particular for  $m_0^2 \ll m_{1/2}^2$ . The CBBN constraint (2.5)—which emerges for  $Y_{\tilde{\tau}_1}$  given by (2.4)—can then be translated into the following  $m_{\tilde{G}}$ -dependent limits [53, 59]:

$$m_{1/2} \geq 0.9 \text{ TeV} \left( \frac{m_{\tilde{G}}}{10 \text{ GeV}} \right)^{2/5} , \quad (2.6)$$

$$T_{\text{R}} \leq 4.9 \times 10^7 \text{ GeV} \left( \frac{m_{\tilde{G}}}{10 \text{ GeV}} \right)^{1/5} , \quad (2.7)$$

where the latter accounts also for  $\Omega_{\tilde{G}} \leq \Omega_{\text{DM}}$ . For  $m_{\tilde{G}}$  at the GeV scale, the lower limit (2.6) then implies heavy colored sparticles that will be difficult to probe at the LHC. As already mentioned above, this provides additional motivation for this work since a SUSY discovery could still be possible via direct stau pair production.

### 2.3 Exceptionally small thermal relic stau abundances

The  $T_{\text{R}}$  limit (2.7) illustrates the mentioned tension with thermal leptogenesis being a viable explanation of the baryon asymmetry in the Universe.<sup>3</sup> In fact, this tension has motivated studies of scenarios with non-standard thermal history in which  $Y_{\tilde{\tau}_1}$  is diluted by significant entropy production after decoupling and before BBN [52, 57, 104] and scenarios with R-parity violation [17] such that (2.5) is respected. Nevertheless, with a standard thermal

---

<sup>3</sup>In scenarios that are less constrained than the CMSSM, the  $T_{\text{R}}$  limit will be more relaxed if the ratio of the masses  $m_{\tilde{g}}$  and  $m_{\tilde{\tau}_1}$  is smaller than  $m_{\tilde{g}}/m_{\tilde{\tau}_1} > 6$  encountered in the  $\tilde{\tau}_1$  LOSP region of the CMSSM [56].



history and R-parity conservation, it has also been found that SUSY models with enhanced stau-Higgs couplings [73, 74] and/or the pattern  $2m_{\tilde{\tau}_1} \simeq m_{H^0}$  between the mass of the stau  $\tilde{\tau}_1$  and the mass of the heavy neutral CP-even Higgs  $H^0$  [74] can lead to particularly efficient primordial stau annihilation and thereby to exceptionally small yields that may respect the CBBN constraint [55]:<sup>4</sup>

$$Y_{\tilde{\tau}_1} \lesssim 2 \times 10^{-15} . \quad (2.8)$$

For such a yield, the  $\tau_{\tilde{\tau}_1}$  limit (2.5) is no longer applicable and the larger values of  $m_{\tilde{G}}$  or  $f_{\text{PQ}}$  are not disfavored such that  $T_{\text{R}} \gtrsim 10^9$  GeV and standard thermal leptogenesis may be viable. For the  $\tilde{G}$  LSP case, also the region  $0.1m_{\tilde{\tau}_1} \lesssim m_{\tilde{G}} < m_{\tilde{\tau}_1}$ , in which the kinematical  $m_{\tilde{G}}$  determination [24] is expected to be viable, is no longer disfavored.

In light of these appealing features, let us recall some aspects of the conditions that lead to enhanced stau-Higgs couplings; see also refs. [73, 74]. (For details and notations of couplings we refer to appendix A.) The stau-Higgs couplings are governed by  $\tan \beta$ ,  $\mu$ , and the trilinear coupling  $A_\tau$  in the stau sector. These parameters determine also the admixture of the left-handed and right-handed gauge eigenstates,  $\tilde{\tau}_L$  and  $\tilde{\tau}_R$ , in the lighter stau mass eigenstate

$$\tilde{\tau}_1 = \cos \theta_{\tilde{\tau}} \tilde{\tau}_L + \sin \theta_{\tilde{\tau}} \tilde{\tau}_R . \quad (2.9)$$

Thereby, there is a relation between the size of the stau-Higgs couplings and the stau mixing angle  $\theta_{\tilde{\tau}}$ . This becomes most explicit in the decoupling limit [105] in which the light CP-even Higgs boson  $h^0$  is much lighter than  $H^0$  and the CP-odd Higgs boson  $A^0$ . Here one finds that the  $\tilde{\tau}_1 \tilde{\tau}_1 h^0$  coupling is proportional to  $\sin 2\theta_{\tilde{\tau}}$  and the off-diagonal term in the stau-mass squared matrix,  $X_\tau = A_\tau - \mu \tan \beta$ , while the  $\tilde{\tau}_1 \tilde{\tau}_1 H^0$  coupling is found to be proportional to  $(A_\tau \tan \beta - \mu) \sin 2\theta_{\tilde{\tau}}$ . Thus, the absolute value of these couplings becomes maximal for  $\theta_{\tilde{\tau}} \rightarrow \pi/4$ , which corresponds to maximal left-right mixing in (2.9), and sizeable for large  $\tan \beta$  and large absolute values of  $\mu$  and/or  $A_\tau$ . In the corresponding parameter regions, on which we focus in this work, one then finds enhanced stau-Higgs couplings and the mentioned efficient stau annihilation that can lead to (2.8).

Here one has to stress that additional theoretical constraints might become important in regions with large stau-Higgs couplings. These regions can be associated with unwanted CCB minima in the scalar MSSM potential [73, 74, 106, 107]. Our electroweak vacuum is then only a local minimum and as such metastable. This will still be a viable scenario if the quantum transition rate to the CCB minimum is so small that the lifetime of our electroweak vacuum exceeds the age of the Universe. By studying the decay of the electroweak vacuum with the usual ‘bounce method’ [108] in an effective potential approach [109], it has been found from a fit in the relevant parameter space that a viable scenario has to respect the following metastability condition [107]:

$$\mu \tan \beta < 76.9 \sqrt{m_{\tilde{L}_3} m_{\tilde{E}_3}} + 38.7 (m_{\tilde{L}_3} + m_{\tilde{E}_3}) - 1.04 \times 10^{-4} \text{ GeV} , \quad (2.10)$$

---

<sup>4</sup>There are other cosmological constraints on  $Y_{\tilde{\tau}_1}$  in addition to the considered CBBN constraints, as briefly mentioned in section 1. The  $Y_{\tilde{\tau}_1}$  limits imposed by these other constraints are typically at most equally restrictive and are usually evaded also for  $Y_{\tilde{\tau}_1}$  satisfying (2.8); cf. section 1 in ref. [74].

where  $m_{\tilde{L}_3}$  and  $m_{\tilde{E}_3}$  are respectively the left-handed and right-handed stau soft-breaking masses. We have checked this condition by explicitly constructing the bounce action for several parameter points and agree within the uncertainty given in [107]. However, this condition is not as rigid as, for example, bounds from direct SUSY particle searches or flavor changing decays since only the exponential contribution to the decay of the electroweak vacuum can be evaluated easily, while a calculation of the full width of the decay into the CCB minimum is highly non-trivial. Nevertheless, scenarios in which an exceptional yield (2.8) results from enhanced stau-Higgs couplings only [73, 74], can be disfavored by the CCB constraint (2.10) if taken at face value (*cf.* sections 5 and 6 and ref. [106]).<sup>5</sup>

In scenarios with  $2m_{\tilde{\tau}_1} \simeq m_{H^0}$ , primordial stau annihilation can proceed efficiently via the  $H^0$  resonance and thereby lead to an exceptionally small  $Y_{\tilde{\tau}_1}$ . Here the annihilation channel  $\tilde{\tau}_1 \tilde{\tau}_1^* \rightarrow b\bar{b}$  turned out to be the most relevant one, which also benefits from enhanced stau-Higgs couplings. However, because of the  $H^0$  resonance, an exceptional yield (2.8) is already possible with more moderate values of  $\tan\beta$ ,  $|\mu|$ , and  $|A_\tau|$  [74]. Thereby, such scenarios can lead to (2.8) and still respect the discussed CCB constraints.

There are additional constraints from B-physics observables and Higgs searches, which can become relevant in parameter regions with sizeable  $\tan\beta$ . In particular, the non-observation of the decay  $B_s \rightarrow \mu^+ \mu^-$  provides an upper limit on the corresponding branching ratio [111]

$$\text{BR}(B_s \rightarrow \mu^+ \mu^-) < 4.3 \times 10^{-8} \text{ @ 95\% CL} , \quad (2.11)$$

which sets stringent limits on the relevant parameter space. Also the measurement of [111]

$$\text{BR}(b \rightarrow s\gamma) = (3.55 \pm 0.33) \times 10^{-4} \quad (2.12)$$

can give relevant constraints. Furthermore, there are constraints on the Higgs sector of the MSSM in scenarios with large  $\tan\beta$  and small  $m_{A^0}$  from Higgs searches in the  $\tau\bar{\tau}$  and  $b\bar{b}$  channels. Most stringent limits are set recently by the LHC experiments [112, 113]. The study in ref. [113], *e.g.*, excludes  $m_{A^0} \lesssim 280$  GeV for  $\tan\beta \gtrsim 50$  in the  $m_h^{\text{max}}$  benchmark scenario (defined *e.g.* in [113]) in the  $\tau\bar{\tau}$  channel. However, as shown in section 6, scenarios with resonant primordial stau annihilation leading to (2.8) can respect these B-physics and collider constraints as well.

In this paper, we investigate whether it can be possible to find manifestations of an exceptionally small yield (2.8) when studying the direct production of quasi-stable staus in current collider experiments. As we will see in the next sections, for this purpose it is crucial to consider not only the Drell–Yan process but to also include the additional channels from  $b\bar{b}$  annihilation and  $gg$  fusion in the cross section calculation.

### 3. Direct production of stau pairs at hadron colliders

In this section we calculate the cross section for direct stau pair production at hadron colliders. We describe the relevant production channels and the methods used in our calculation.

---

<sup>5</sup>In a recent updated study [110] the authors of [106] also included collider implication of the cosmological motivated  $2m_{\tilde{\tau}_1} \approx m_{H^0}$  resonance region. However, they did not consider the additional  $b\bar{b}$  and  $\gg$  direct production channels discussed in this work.

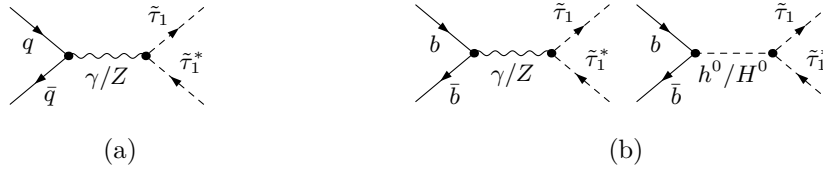


**Figure 1:** Feynman diagrams for stau pair production (a) via the Drell–Yan process and (b) via  $b\bar{b}$  annihilation. Here,  $q = u, d, c, s$ .

tions. Numerical results are shown to illustrate the dependence on the SUSY parameters and to provide predictions for the Tevatron and the LHC. The obtained cross sections are independent of the stau lifetime.

Within the MSSM, stau pairs can be produced directly at hadron colliders,

$$pp(p\bar{p}) \rightarrow \tilde{\tau}_i \tilde{\tau}_j^*, \quad (3.1)$$

where  $\tilde{\tau}_{i,j}$  denotes any of the two stau mass eigenstates. After electroweak symmetry breaking the soft-breaking terms in the MSSM Lagrangian induce a mixing among the particles of identical color and electric charge. In the sfermion sector, left-handed and right-handed gauge eigenstates mix to form mass eigenstates, see appendix A. The mixing is proportional to the mass of the SM partner fermion and can thus be sizeable for sleptons of the third generation. In the following, we concentrate on the production of the lighter  $\tilde{\tau}_1 \tilde{\tau}_1^*$  pairs. Results for  $\tilde{\tau}_2 \tilde{\tau}_2^*$  and  $\tilde{\tau}_1 \tilde{\tau}_2^*$  production can be obtained in close analogy. Their production cross sections, however, are suppressed by the heavier  $\tilde{\tau}_2$  mass.

### 3.1 Direct $\tilde{\tau}_1 \tilde{\tau}_1^*$ production channels

At hadron colliders typically the leading contribution to direct  $\tilde{\tau}_1 \tilde{\tau}_1^*$  production arises from the  $q\bar{q}$  induced Drell–Yan type process at  $\mathcal{O}(\alpha^2)$ , see figure 1 (a). The Drell–Yan production cross section depends only on the stau mass  $m_{\tilde{\tau}_1}$  and the stau mixing angle  $\theta_{\tilde{\tau}}$ .

Stau pairs can also be produced from  $b\bar{b}$  annihilation, mediated by the neutral gauge bosons ( $\gamma$ ,  $Z$ ) and by the neutral CP-even Higgs bosons ( $h^0$ ,  $H^0$ ), at the same order of perturbation theory. The corresponding Feynman diagrams are displayed in figure 1 (b). This channel is suppressed by the low bottom-quark density inside protons, but can be enhanced by on-shell Higgs propagators and by the bottom-Higgs and the stau-Higgs couplings in certain regions of the SUSY parameter space. Note that the CP-odd Higgs and Goldstone bosons,  $A^0$  and  $G^0$ , do not couple to a diagonal  $\tilde{\tau}_i \tilde{\tau}_i^*$  pair at tree-level and, in absence of CP violating effects in the MSSM, there is also no induced mixing between the CP-even and the CP-odd Higgs boson states at higher orders of perturbation theory. The  $A^0$  and  $G^0$  bosons thus do not enter our calculation.

Gluon-induced  $\tilde{\tau}_1 \tilde{\tau}_1^*$  production is only possible at the one-loop level, mediated by a quark or squark loop, as shown in figure 2. Even though these contributions are formally of higher orders,  $\mathcal{O}(\alpha_s^2 \alpha^2)$ , they can give sizeable contributions at the proton-proton machine LHC at high center-of-mass energies where the  $gg$  luminosity is significantly higher than the  $q\bar{q}$  luminosity.

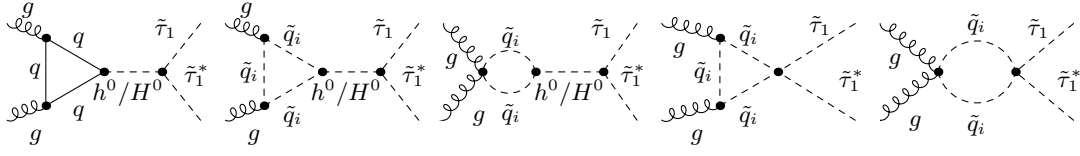


**Figure 2:** Feynman diagrams for the gluon fusion contribution to stau pair production. The quarks  $q$  and squarks  $\tilde{q}_i$ ,  $i = 1, 2$ , running in the loops can be of any flavor.

Let us note again that the additional  $b\bar{b}$  and  $gg$  channels are not included in the general purpose Monte Carlo event generators like `Pythia` [85] or `Herwig` [86]. We use the programs `FeynArts` 3.6 [114] and `FormCalc` 7.0 with `LoopTools` 2.6 [115] to generate and calculate the amplitudes corresponding to the Feynman diagrams of figures 1 and 2. The Higgs boson masses and the  $H^0$  width are computed with `FeynHiggs` 2.7.4 [116]. We include QCD and SUSY-QCD corrections at NLO for the Drell–Yan channel predictions calculated with `Prospino` 2, by scaling our cross sections with the respective  $K$ -factors,  $K \equiv \sigma_{\text{NLO}}/\sigma_{\text{LO}}$ . Furthermore, we use a resummed effective  $b\bar{b}h^0/b\bar{b}H^0$  vertex for the gluon fusion and  $b\bar{b}$  contributions, as explained below and in appendix B.

We do not include higher-order QCD and SUSY-QCD corrections to the Higgs-mediated channels. These are expected to be positive and similar to the results for on-shell Higgs production, see [117] and references therein. In this way our analysis gives a conservative estimate of the enhancement effects from the  $b\bar{b}$  and gluon fusion production channels. Note also that additional contributions to the direct  $\tilde{\tau}_1 \tilde{\tau}_1^*$  production can arise from  $W^+W^-$  fusion. Those however would be smaller by at least one order of magnitude compared to the other channels [82] and are not included in our analysis.

As motivated in section 2, we are particularly interested in parameter regions with enhanced stau–Higgs couplings and thus typically in scenarios with large  $\tan\beta$ . It has been known for a long time [118–122] that radiative corrections to the  $b\bar{b}h^0/b\bar{b}H^0$  vertex can be important especially for large  $\tan\beta$  and drive down the cross section compared to the tree-level result. As shown in [122, 123] the leading  $\tan\beta$ -enhanced corrections can be resummed to all orders in perturbation theory by using an appropriate effective bottom-quark mass,  $m_b^{\text{eff}}$ , and effective  $b\bar{b}h^0/b\bar{b}H^0$  couplings. We adopt this approach, as explained in detail in appendix B.

At hadron colliders, the gluon-fusion and  $b\bar{b}$ -annihilation processes with an  $s$ -channel Higgs boson can become resonant in regions of the SUSY parameter space in which the Higgs boson is heavier than the two produced staus. For intermediate  $\tilde{\tau}_1$  masses respecting the robust LEP limit  $m_{\tilde{\tau}_1} \geq 82$  GeV [14], the lighter CP-even Higgs boson,  $h^0$ , is expected to be too light to go on-shell ( $m_{h^0} < 140$  GeV, *e.g.*, [124]). This is different for the heavier  $H^0$  boson. In parameter regions with  $m_{H^0} \geq 2m_{\tilde{\tau}_1}$  we therefore include the total decay width of the  $H^0$  boson,  $\Gamma_{H^0}^0$  in the propagator,

$$\frac{1}{p^2 - m_{H^0}^2} \longrightarrow \frac{1}{p^2 - m_{H^0}^2 + im_{H^0}\Gamma_{H^0}^0}.$$

### 3.2 Numerical results

Let us now investigate direct  $\tilde{\tau}_1 \tilde{\tau}_1^*$  production at hadron colliders numerically. Our focus is on the impact of the  $b\bar{b}$ -annihilation and the gluon-fusion channels in comparison to the Drell–Yan process.

The cross section for direct stau production depends mainly on  $m_{\tilde{\tau}_1}$ ,  $m_{H^0}$ ,  $\tan\beta$ , and on  $\theta_{\tilde{\tau}}$  (or equivalently on  $\mu$  and  $A_{\tau}$ ). It also depends on the  $H^0$  boson width,  $\Gamma_{H^0}$ , and thus indirectly on the SUSY mass spectrum. In addition, squark masses enter indirectly via the loops in the gluon-fusion channel and, as does the trilinear coupling  $A_t$  in the stop sector, via the effective bottom couplings.

We use the following input parameters in our numerical study. As a starting point, we choose a  $\tilde{\tau}_1$ -LOSP scenario with moderate squark masses and a large stau–Higgs coupling, fixed by the following soft-breaking parameters at the low scale:

$$\begin{aligned} M_1 = M_2 = M_3 = 1.2 \text{ TeV}, \quad A_t = A_b = A_{\tau} = 600 \text{ GeV}, \\ m_{\tilde{Q}_i} = m_{\tilde{U}_i} = m_{\tilde{D}_i} = 1 \text{ TeV}, \quad m_{\tilde{L}_{1/2}} = m_{\tilde{E}_{1/2}} = 500 \text{ GeV}, \end{aligned} \quad (3.2)$$

where  $M_i$  denote the gaugino mass parameters associated with the SM gauge groups  $U(1)_Y$ ,  $SU(2)_L$ , and  $SU(3)_c$ ,  $m_{\tilde{Q}_i}$  ( $m_{\tilde{U}_i}$  and  $m_{\tilde{D}_i}$ ) the left-handed (right-handed) squark soft-breaking masses,  $m_{\tilde{L}_{1/2}}$  ( $m_{\tilde{E}_{1/2}}$ ) the left-handed (right-handed) slepton soft-breaking masses for the first two generations, and  $A_b$  the trilinear coupling in the sbottom sector. If not stated otherwise, we choose

$$\begin{aligned} \theta_{\tilde{\tau}} = 45^\circ, \quad m_{\tilde{\tau}_1} = 200 \text{ GeV}, \\ \tan\beta = 30, \quad \mu = 500 \text{ GeV}, \quad m_A = 400 \text{ GeV}, \end{aligned} \quad (3.3)$$

as inputs for the third-generation sleptons, as discussed in appendix A, and for the Higgs-sector, where  $m_A$  denotes the mass of the CP-odd Higgs boson  $A^0$ . With these parameters, the considered scenario falls into the decoupling limit of the MSSM [105] where  $m_{H^0} \approx m_A$ . Note that the chosen value of  $\tan\beta$  (and also of  $\mu$ ) is rather moderate compared to the cosmologically motivated scenarios considered in ref. [74] and discussed in section 2.3.

From the input parameters (3.2) and (3.3), we calculate the physical MSSM parameters using tree-level relations for sfermions, neutralinos, and charginos. Physical masses are then passed to **Prospino 2** to calculate the Drell–Yan  $K$ -factors at NLO in QCD and SUSY-QCD. The NLO corrections to the Drell–Yan channel typically amount to 20–40% in the considered parameter space.

SM input parameters are chosen according to [14]

$$\begin{aligned} M_Z = 91.1876 \text{ GeV}, \quad M_W = 80.4248 \text{ GeV}, \quad G_F = 1.1664 \times 10^{-5} \text{ GeV}, \\ m_b^{\overline{\text{MS}}}(M_Z) = 2.936 \text{ GeV}, \quad m_t = 173.1 \text{ GeV}, \quad m_{\tau} = 1.776 \text{ GeV}. \end{aligned} \quad (3.4)$$

We include the MSTW08LO [125] set of parton distribution functions (PDFs) and use the running strong coupling constant  $\alpha_s(\mu_R)$  they provide. Factorization and renormalization scales are set to the mass of the produced stau  $\mu_R = \mu_F = m_{\tilde{\tau}_1}$ .

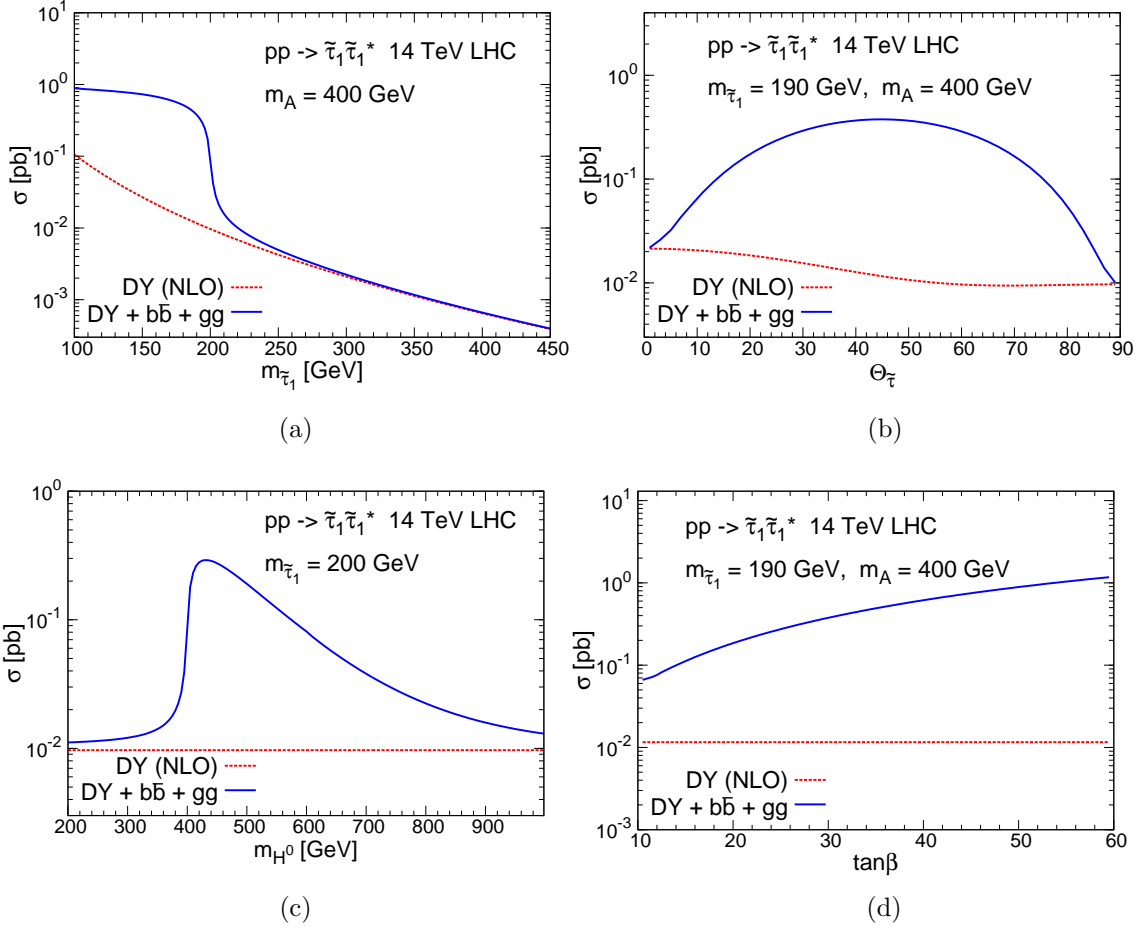


**Figure 3:** Cross section of direct  $\tilde{\tau}_1\tilde{\tau}_1^*$ -pair production (solid lines, blue) and the Drell–Yan prediction (dashed lines, red) at the LHC with  $\sqrt{S} = 14$  TeV as a function of (a)  $m_{\tilde{\tau}_1}$ , (b)  $\theta_{\tilde{\tau}}$ , (c)  $m_{H^0}$ , and (d)  $\tan\beta$ . No kinematical cuts are applied. SUSY input parameters are as given in (3.2) and (3.3) if not varied or unless stated otherwise in the legend of the respective panel. Note that  $m_{H^0} \approx m_A$  (decoupling limit) holds in most of the shown regions.

At this point we want to mention again that our calculation of the  $b\bar{b}$  and  $gg$  channels is formally at LO. By using an effective bottom-quark mass,  $m_b^{\text{eff}}$ , and effective  $b\bar{b}h^0/b\bar{b}H^0$  couplings, however, the dominant  $\tan\beta$  enhanced corrections are included in our results. Nevertheless, we do not consider non- $\tan\beta$  enhanced higher-order corrections, and the remaining renormalization and factorization scale dependence yields a possibly large theoretical uncertainty to our cross section predictions. A more detailed study at NLO would be desirable, taking also uncertainties due to the dependence on the PDF set, and the bottom-quark PDF in particular, into account.

In figure 3 we show the direct production cross section for  $\tilde{\tau}_1\tilde{\tau}_1^*$  pairs at the LHC with  $\sqrt{S} = 14$  TeV as a function of (a)  $m_{\tilde{\tau}_1}$ , (b)  $\theta_{\tilde{\tau}}$ , (c)  $m_{H^0}$ , and (d)  $\tan\beta$ . The remaining SUSY parameters are basically fixed according to (3.2) and (3.3). In figures 3(b) and (d), we move to  $m_{\tilde{\tau}_1} = 190$  GeV, where stau production is possible via on-shell  $H^0$  exchange. The

dashed (red) lines show the Drell–Yan (DY) cross section at NLO, whereas the solid (blue) lines include the additional  $b\bar{b}$  and  $gg$  contributions. The Drell–Yan cross section depends only on  $m_{\tilde{\tau}_1}$  and  $\theta_{\tilde{\tau}}$ , as already mentioned above. It decreases strongly for increasing  $\tilde{\tau}_1$  masses and varies with  $\theta_{\tilde{\tau}}$  by a factor that can be at most slightly larger than 2. As shown in figure 3 (b), this factor takes on its largest value for  $\theta_{\tilde{\tau}} \approx 0$ , *i.e.*, for an almost left-handed  $\tilde{\tau}_1$ . The factor of  $\approx 2$  difference between the Drell–Yan cross sections at  $\theta_{\tilde{\tau}} \approx 0$  and  $\theta_{\tilde{\tau}} \approx \pi/2$  is determined mainly by different gauge couplings of the left-handed and right-handed states. It is almost independent of kinematics and hardly effected when going from  $\sqrt{S} = 14$  TeV to 7 TeV.

The impact of the  $b\bar{b}$  and  $gg$  channels depends strongly on the mass hierarchy between  $\tilde{\tau}_1$  and  $H^0$ , as can clearly be seen in figures 3 (a) and (c). If  $m_{H^0} > 2m_{\tilde{\tau}_1}$ , these additional channels can change the direct production cross section by more than one order of magnitude with respect to the Drell–Yan result. At the threshold  $m_{H^0} = 2m_{\tilde{\tau}_1}$ , the  $b\bar{b}$  and  $gg$  contributions drop steeply and are only marginally important for  $m_{H^0} \ll 2m_{\tilde{\tau}_1}$ .

Figures 3 (b) and (d) illustrate the dependence of the total direct production cross section on the parameters  $\theta_{\tilde{\tau}}$  and  $\tan\beta$  that govern the stau-Higgs-coupling strength. Here, the total direct production cross section is dominated by on-shell Higgs production. Thus, the dependence on  $\theta_{\tilde{\tau}}$  and  $\tan\beta$  reflects the  $\tilde{\tau}_1\tilde{\tau}_1^*H^0$  coupling, discussed in section 2.3 and given in appendix A.2. As shown there and illustrated here, this coupling is basically proportional to  $\sin 2\theta_{\tilde{\tau}}$  and also to  $\tan\beta$  (or more precisely to  $A_{\tau}\tan\beta$ ). The additional contributions from the  $b\bar{b}$  and  $gg$  channels are tiny in cases of very small mixing,  $\theta_{\tilde{\tau}} \rightarrow 0, \pi$ . The exact position of the minimum depends on the relative importance of the  $\tilde{\tau}_1\tilde{\tau}_1^*H^0$  and  $\tilde{\tau}_1\tilde{\tau}_1h^0$  couplings, and can be slightly above/below  $\theta_{\tilde{\tau}} = 0, \pi$ , see also (A.9).

In turn, they become most important for maximal mixing, *i.e.*, at  $\theta_{\tilde{\tau}} \approx \pi/4$ . There, the additional contributions push up the total direct production cross section by up to two orders of magnitude for very large  $\tan\beta$  and are already sizeable for small  $\tan\beta$ .

Let us now turn to a scenario where the  $H^0$  is very heavy and thus almost decoupled,  $m_{H^0} = 1$  TeV. We again investigate the dependence of the total cross section on  $\theta_{\tilde{\tau}}$  and  $\tan\beta$ , shown in figure 4. We focus on parameters that allow for enhanced  $\tilde{\tau}_1\tilde{\tau}_1^*h^0$  couplings, *i.e.* large values for  $\mu$  and  $\tan\beta$ . In figure 4 (a) we consider  $\mu = 800$  GeV and  $\tan\beta = 50$  while the other parameters are fixed according to (3.2) and (3.3). Again, the contribution from the additional  $b\bar{b}$  and  $gg$  channels can be sizeable. The enhancement amounts to a factor between two and three when considering very large values of  $\tan\beta$  and maximal mixing  $\theta_{\tilde{\tau}} \approx \pi/4$ . Here dominant contributions come mainly from off-shell  $h^0$  exchange together with large stau-Higgs couplings. Thus, the relative importance between the  $gg$  channel and the  $b\bar{b}$  channel can be different compared to situations with dominant contributions from on-shell  $H^0$  exchange since the two Higgses couple differently to the quark and squark loops. Clearly, for a larger contribution of the loop-induced  $gg$  channel, a stronger dependence on the squark masses is introduced in our calculation. This does not only concern the overall mass scale but also the mass splitting between the squarks, as is well known for on-shell Higgs production via gluon fusion, see [124] and references therein. For example, contributions from squark loops get small when squarks within one generation are almost degenerate. Additionally, slight enhancements in the  $gg$  channel can

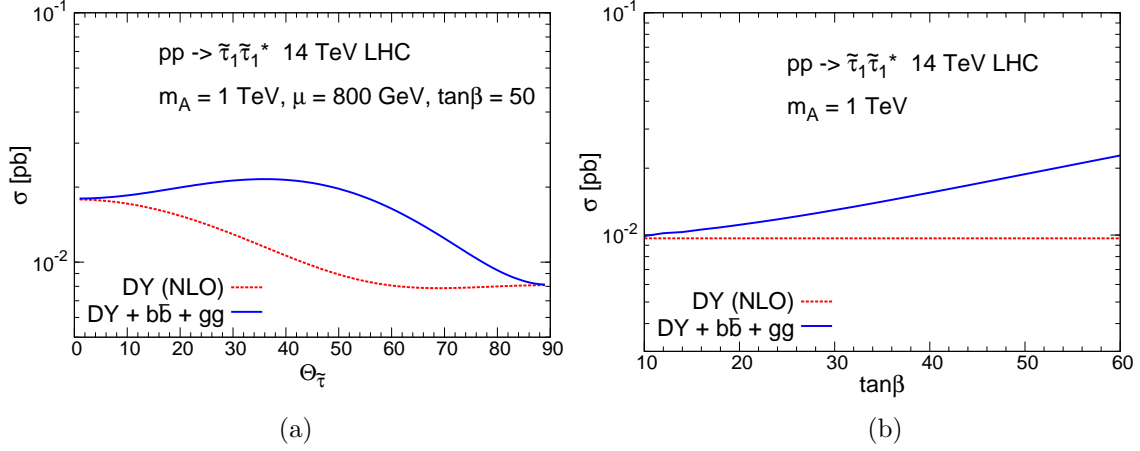


**Figure 4:** Cross section of direct  $\tilde{\tau}_1 \tilde{\tau}_1^*$ -pair production (solid lines, blue) and the Drell–Yan prediction (dashed lines, red) at the LHC with  $\sqrt{S} = 14$  TeV as a function of (a)  $\theta_{\tilde{\tau}}$  and (b)  $\tan\beta$ . No kinematical cuts are applied. SUSY input parameters as given in (3.2) and (3.3) if not varied or stated otherwise. Note that here  $m_{H^0} \approx m_A = 1$  TeV (decoupling limit).

appear at thresholds where the resonance requirement  $2m_{\tilde{q}} \approx m_{H^0}$  is fulfilled between squarks in the loops and the heavy Higgs  $H^0$ , as shown in ref. [84]. We want to note that, despite the large couplings, all parameter points considered above are in agreement with the CCB constraint (2.10).

We summarize the potential impact of the  $b\bar{b}$  and  $gg$  channels for the SUSY scenario defined in (3.2) and (3.3) again in figure 5, where the Drell–Yan predictions (dashed lines) and the full cross sections (solid lines) are shown for  $\tilde{\tau}_1 \tilde{\tau}_1^*$  production at the LHC for  $\sqrt{S} = 14$  TeV (top, red) and for 7 TeV (middle, blue). When going down from 14 TeV to 7 TeV, the cross section decreases by up to about a factor of 5. The relative importance of the  $b\bar{b}$  and  $gg$  channels however are similarly important in the region where on-shell  $H^0$  exchange contributes. Thus, for both  $\sqrt{S} = 7$  TeV and 14 TeV, the  $b\bar{b}$  and  $gg$  channels should not be neglected in a precise cross section prediction. We also show the direct  $\tilde{\tau}_1 \tilde{\tau}_1^*$  production cross section expected at the Tevatron with  $\sqrt{S} = 1.96$  TeV (bottom, green). Due to the higher parton momentum fractions  $x$  needed at the Tevatron, the gluon and the  $b\bar{b}$  luminosities are reduced compared to the LHC case. Accordingly, the respective  $gg$  and  $b\bar{b}$  contributions to direct stau production are only small, as illustrated.

#### 4. Collider phenomenology with directly produced long-lived staus

In this section we focus on scenarios with long-lived staus, *i.e.*,  $\tau_{\tilde{\tau}_1} \gtrsim 10^{-6}$  s. At collider experiments, pair production of long-lived staus will give a clear CHAMP signal in the detectors if kinematical cuts are applied to discriminate between signal and muon background. Here, we study the impact of these kinematical cuts on the direct production cross section prediction and differential distributions. We show that experimental observation of direct stau production could provide important insights into the SUSY model realized in nature. For particularly well-motivated cosmological scenarios, we find that relatively large



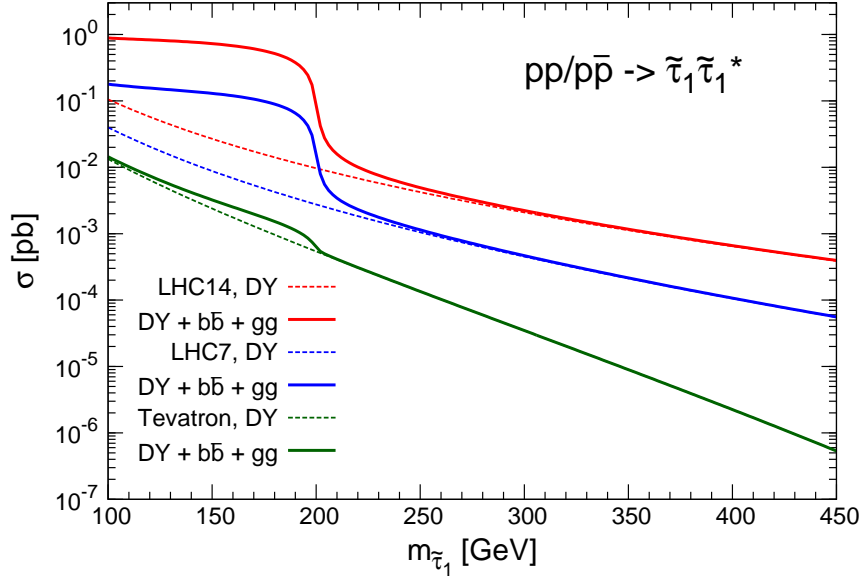


**Figure 5:** Direct  $\tilde{\tau}_1 \tilde{\tau}_1^*$ -pair production cross sections as a function of  $m_{\tilde{\tau}_1}$  for the SUSY scenario with (3.2) and (3.3) at the LHC with  $\sqrt{S} = 14$  TeV (top, red) and 7 TeV (middle, blue) and the Tevatron with  $\sqrt{S} = 1.96$  TeV (bottom, green). The Drell–Yan predictions are shown by the dashed lines and the full cross section, including  $b\bar{b}$  and  $gg$  channels, by the solid lines.

numbers of staus are expected to get stopped already in the main detectors at the LHC. Thereby, analyses of stau decays may become a viable tool to identify the LSP and/or to probe high scales such as the Planck scale  $M_{\text{Pl}}$  or the Peccei–Quinn scale  $f_{\text{PQ}}$  in the laboratory.

#### 4.1 Kinematical cuts

For a realistic experimental analysis, we need to include kinematical cuts on the phase space of the staus to reduce possible backgrounds to the CHAMP signal. The signature of a CHAMP traversing a detector is a slowly moving minimal ionising particle with high transverse-momentum  $p^{\text{T}}$ . In the experiments, this results in a long time-of-flight (TOF) and an anomalously large ionization-energy loss rate ( $dE/dx$ ) [126]. Since the CHAMP loses energy primarily through low-momentum-transfer interactions, it will be highly penetrating and will likely be reconstructed as a muon [97]. At hadron colliders, experimental CHAMP searches have been performed by the CDF [97] and the D0 [96] collaborations at the Tevatron and are planned at the LHC in the near future [127]. In accordance with those analyses, we apply the following kinematical cuts on the produced staus:

$$\begin{aligned} p^{\text{T}} &> 40 \text{ GeV}, & 0.4 < \beta < 0.9, \\ |\eta| < 0.7 \text{ (Tevatron)}, & |\eta| < 2.4 \text{ (LHC)}, \end{aligned} \quad (4.1)$$

where the cuts have to be fulfilled by at least one of the  $\tilde{\tau}_1$ ’s. Here  $\eta = -\ln(\tan \theta/2)$  is the pseudo-rapidity and  $\beta = |\mathbf{p}|/E$  the stau velocity. This should reduce the background from very slow moving muons to a negligible level [128].

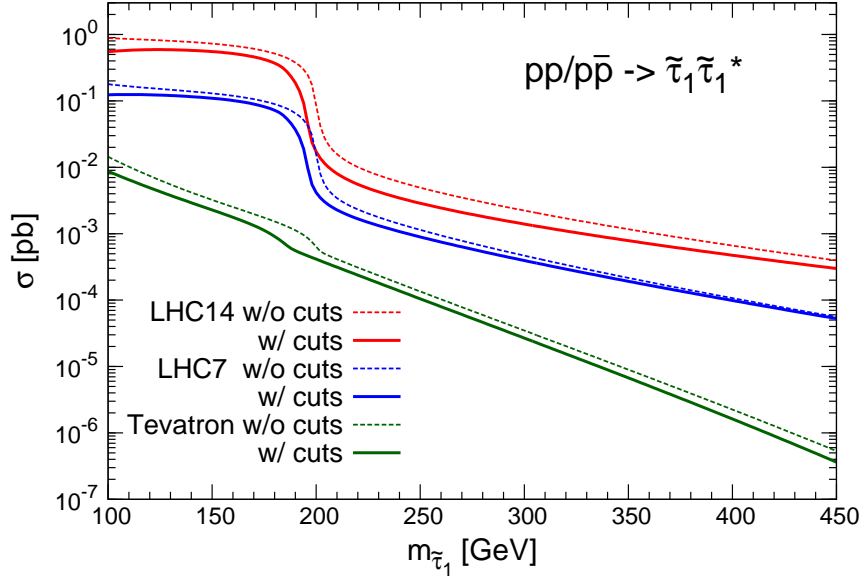


**Figure 6:** Direct  $\tilde{\tau}_1 \tilde{\tau}_1^*$ -pair production cross sections before (dashed lines) and after (solid lines) application of the kinematical cuts (4.1) as a function of  $m_{\tilde{\tau}_1}$  for the SUSY scenario with (3.2) and (3.3) at the LHC with  $\sqrt{S} = 14$  TeV (top, red) and 7 TeV (middle, blue) and the Tevatron with  $\sqrt{S} = 1.96$  TeV (bottom, green).

For our theoretical predictions, we use the same inputs as in section 3. In particular, we include the inclusive NLO  $K$ -factors provided by **Prospino 2** for the Drell–Yan channel, also when cuts are applied. Since QCD and SUSY-QCD corrections only effect the hadronic part of the considered  $\tilde{\tau}_1 \tilde{\tau}_1^*$  production, the cut dependence of the  $K$ -factors is expected to be small. Note that we furthermore assume here direct  $\tilde{\tau}_1 \tilde{\tau}_1^*$  production to be the dominant  $\tilde{\tau}_1$  production source and do not include  $\tilde{\tau}_1$ ’s resulting from cascade decays in our signal definition. Otherwise, an additional jet and/or lepton veto can be used to separate directly produced staus from ones produced at the end of a decay chain. We will briefly investigate the relative importance of these concurrent production mechanisms for representative CMSSM benchmark scenarios in section 5.2.

In figure 6 we compare the full direct production cross sections with (solid lines) and without (dashed lines) the kinematical cuts (4.1) applied as a function of  $m_{\tilde{\tau}_1}$  for the LHC with  $\sqrt{S} = 14$  TeV (top, red) and 7 TeV (middle, blue) and the Tevatron with  $\sqrt{S} = 1.96$  TeV (bottom, green). At the LHC, the cuts shift the excess slightly away from the  $H^0$  threshold and towards smaller values of  $m_{\tilde{\tau}_1}$  and reduce the overall cross section by some tens of percent. The reduction is stronger at the Tevatron, where in particular the  $b\bar{b}$  and  $g\bar{g}$  channel contributions get cut significantly, so that the Drell–Yan channel provides a good approximation for the full cross section.

Assuming the produced  $\tilde{\tau}_1$ ’s to be stable on the scale of the detectors, our results for the Tevatron shown in figure 6 can directly be compared with the CHAMP cross-section limit from the CDF collaboration [97] given in (2.2). This comparison does not allow to exclude any  $m_{\tilde{\tau}_1} > 100$  GeV for the considered parameters. Nevertheless, smaller masses,

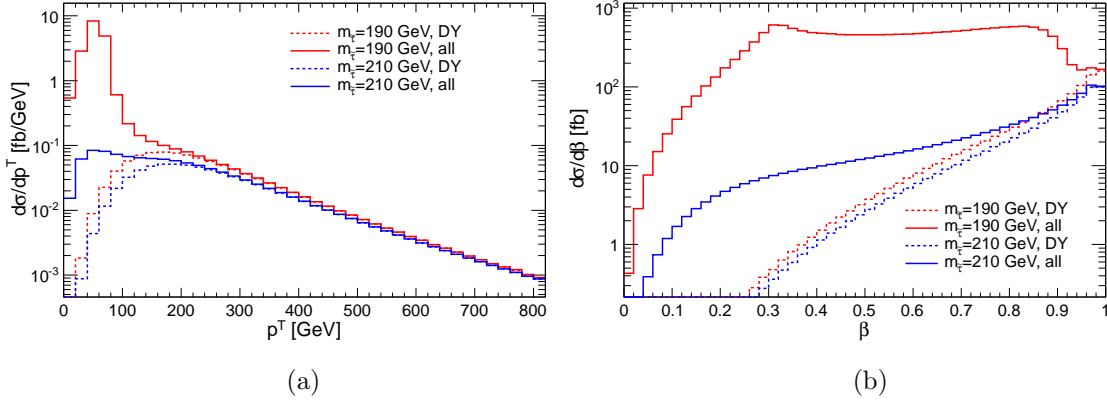


**Figure 7:** (a) Transverse momentum  $p^T$  and (b) velocity  $\beta = |\mathbf{p}|/E$  distributions of direct  $\tilde{\tau}_1 \tilde{\tau}_1^*$ -pair production at the LHC with  $\sqrt{S} = 14$  TeV. The Drell-Yan predictions are shown by dashed lines and the full cross sections, including  $b\bar{b}$  and  $gg$  channels, by solid lines. We consider  $m_{\tilde{\tau}_1} = 190$  GeV (red line) and  $m_{\tilde{\tau}_1} = 210$  GeV (blue line), whereas the other SUSY input parameters are as given in (3.2) and (3.3).

allowed by the conservative LEP limit (2.1),  $82 \text{ GeV} < m_{\tilde{\tau}_1} < 100 \text{ GeV}$ , can be in tension with this limit. However, any robust exclusion would require a full simulation including detector effects, which we do not perform here. Additional indirect stau-pair production mechanisms are not expected to alter this statement considerably since, as discussed above, they would contribute to a different signal region containing jets/leptons.

Dedicated studies of the LHC experiments are announced for the near future. Because of the increased cross section at the LHC, they will probe in detail large parts of the small- $m_{\tilde{\tau}_1}$  parameter space, where the stau can be produced via on-shell  $H^0$  exchange with only a relatively small amount of integrated luminosity already for  $\sqrt{S} = 7$  TeV. In fact, the experiments at the LHC have already performed searches for stable massive particles [129,130]. However, those studies have searched for stable massive particles in the trackers and calorimeters. In those parts of the detectors, the sensitivity to color-singlet particles, such as the  $\tilde{\tau}_1$ , is reduced [129], and findings have only been interpreted for colored massive particles [129,130].

So far we have concentrated on the integrated cross section. To further illustrate the importance of the  $b\bar{b}$  and  $gg$  channel contributions and to investigate the impact of the cuts (4.1) on the different channels, we show the differential distributions with respect to transverse momentum  $p^T$  and the velocity  $\beta$  of the directly produced staus in figure 7. We give results for the LHC with  $\sqrt{S} = 14$  TeV only, however, results for the LHC with  $\sqrt{S} = 7$  TeV are qualitatively identical. We use the basic parameter inputs (3.2) and (3.3) and consider two distinct scenarios,  $m_{\tilde{\tau}_1} = 190$  GeV (red line) and  $m_{\tilde{\tau}_1} = 210$  GeV (blue line). Here, it is  $m_{H^0} = 400$  GeV, *i.e.*, in the first scenario the intermediate  $H^0$  boson can go on-shell while it can only be produced off-shell in the second scenario. We apply the cut  $|\eta| < 2.4$  on the pseudo-rapidity of one of the staus to ensure that not both of the pair-produced staus leave the detector outside of the sensitive region. Cuts on  $p^T$  and  $\beta$  are not applied to be independent of a specific choice of cuts. Also, their potential individual

impact can be inferred directly from figure 7.

We show the Drell–Yan-cross-section prediction (dashed lines) now without any  $K$ -factors and the full cross section including also the  $b\bar{b}$  and  $gg$  channel contributions (solid lines). Clearly, in both scenarios, staus produced in  $b\bar{b}$  and  $gg$  channels are softer and slower than their counterparts from the Drell–Yan-type production. The  $p^T$  distributions for the Drell–Yan channel peak at around  $m_{\tilde{\tau}_1}$  and only few staus are produced with very low  $p^T$ . In contrast, the  $b\bar{b}$  and  $gg$  channel contributions peak for low  $p^T$  and fall off rapidly. The velocity distributions for pure Drell–Yan production rise towards fast moving staus,  $\beta \approx 1$ , while adding the  $b\bar{b}$  and  $gg$  channels results in a rather flat distribution for intermediate values of  $\beta$ . This behavior is more pronounced for scenarios in which an on-shell  $H^0$  exchange is possible (red lines) since here the relative importance of the  $b\bar{b}$  and  $gg$  channels with respect to the Drell–Yan channel is higher. In the case with  $2m_{\tilde{\tau}_1} \gtrsim m_{H^0}$  with  $2m_{\tilde{\tau}_1}$  still very close to  $m_{H^0}$  (blue lines), the  $b\bar{b}$  and  $gg$  channels still contribute significantly and generate a large amount of events with very slow staus.

At this point we want to comment again on scenarios with a heavy, decoupled  $H^0$  boson such as those considered in figure 4. The contributions from  $H^0$ -boson-mediated processes are suppressed in this case, and the same is true if the  $H^0$  boson is far off-shell ( $m_{H^0} \ll 2m_{\tilde{\tau}_1}$ ). Still, the  $b\bar{b}$  and  $gg$  channels can be sizeable if  $h^0$ -mediated processes are important. For large  $\tilde{\tau}_1 \tilde{\tau}_1^* h^0$  couplings (large left-right mixing, large  $|\mu| \tan \beta$  and/or large  $|A_\tau|$ ), we find that the additional production mechanisms, and predominantly the  $gg$ -fusion channel, can give cross section contributions of the same order of magnitude as the Drell–Yan induced process. The shapes of the corresponding  $p^T$  and  $\beta$  distributions are found to be similar to those of the Drell–Yan prediction but have a slightly softer  $p^T$  spectrum.

To summarize, cuts on  $p^T$  or  $\beta$  affect the three production channels to a very different extent and thus change the relative importance of each of the contributions considerably. If the cuts (4.1) are applied, large parts of the additional  $b\bar{b}$  and  $gg$  channel contributions can be lost. We therefore recommend to relax these cuts in future experimental searches to increase the sensitivity especially for cosmological motivated scenarios with  $2m_{\tilde{\tau}_1} \approx m_{H^0}$ , even when this implies that increased backgrounds have to be taken into account. A more detailed study of the interplay between different cut values and expected backgrounds would be required but is beyond the scope of this paper.<sup>6</sup>

## 4.2 Prospects for SUSY parameter determination

In this subsection we want to demonstrate how one could use the fact that the Drell–Yan production cross section depends only on the stau mass and mixing angle, whereas the  $b\bar{b}$  and  $gg$  channels also depend on other SUSY parameters. In fact, the interplay of the Drell–Yan cross section and the additional channels might turn out to be helpful to determine SUSY parameters.

---

<sup>6</sup>Here we would like to refer to the recent paper on direct stau production at the LHC by Heisig and Kersten [131] which appeared during the final stage of our work. In ref. [131], the authors focus on the Drell–Yan-production mechanism and study the LHC discovery potential by performing a Monte Carlo analysis of the signal and the main dimuon background.

If signals of a quasi-stable stau are observed at the LHC, one of the first measurements will be the determination of the stau mass  $m_{\tilde{\tau}_1}$  by using TOF data from the muon chambers. The expected accuracy of this  $m_{\tilde{\tau}_1}$  measurement has been estimated to be  $< 1\%$  [23, 26]. With such a precise knowledge of  $m_{\tilde{\tau}_1}$ , there are high hopes that further SUSY parameters can be extracted from the cross section and differential distributions by comparing experimental results and theoretical predictions. Clearly, these measurements are possible in the case of decay chains with several MSSM particles involved [26, 31–39]. However, in the following we present ideas how such measurements could also be possible just from direct production. To disentangle those channels, appropriate jet and/or lepton vetos are assumed. Moreover, the measurements require more integrated luminosity than needed for a potential stau discovery.

First of all, once the stau mass is known, the Drell–Yan production cross section can be given as a function of the stau mixing angle  $\theta_{\tilde{\tau}}$  alone. If also the direct stau production cross section can be identified experimentally, this will allow us to determine  $\theta_{\tilde{\tau}}$  in a scenario in which the stau pair production cross section is governed by the Drell–Yan channel. As shown in figures 3(b) and 4(a) and as already discussed, the Drell–Yan cross section is maximal in case of an almost purely left-handed  $\tilde{\tau}_1$  and minimal for  $\theta_{\tilde{\tau}} \approx \pi/2$ . An excess of the experimentally obtained cross section over the Drell–Yan expectation at  $\theta_{\tilde{\tau}} \approx \pi/2$  would thus point to  $\theta_{\tilde{\tau}} < \pi/2$  and non-negligible mixing between the left-handed and right-handed eigenstates in Drell–Yan-channel-dominated scenarios. Furthermore, a sizeable deviation from  $\theta_{\tilde{\tau}} \approx \pi/2$  may support also the hypothesis that the observed CHAMP is indeed a stau and not a quasi-stable dominantly right-handed selectron or smuon.

However, in general, a larger experimentally obtained cross section compared to the minimal Drell–Yan expectation for a certain mass could imply both  $\theta_{\tilde{\tau}} < \pi/2$  or also sizeable contributions from  $b\bar{b}$  annihilation and  $gg$  fusion; *cf.* figures 3(b) and 4(a). On the other hand, a significant excess of the measured cross section over the maximal Drell–Yan cross section prediction may provide a first hint for the importance of the  $b\bar{b}$ -annihilation and  $gg$ -fusion processes calculated in this work; see also section 6 below.

These possible ambiguities in the interpretation of experimental findings on the integrated cross section could be resolved by studying also the differential distributions. As we have seen above, the  $p^T$  and  $\beta$  distributions differ strongly from the Drell–Yan prediction when the  $b\bar{b}$  and  $gg$  channels are important. From the shape of the experimentally measured distributions, one could then be able to determine whether the Drell–Yan channel or the other channels give the dominant contribution to the production cross section. Also the distribution with respect to the invariant mass of the produced stau pair,  $m_{\tilde{\tau}_1\tilde{\tau}_1^*}$ , can be helpful for this purpose. In fact, the invariant mass distribution might allow even for the determination of the mass  $m_{H^0}$  and the width  $\Gamma_{H^0}$  of the  $H^0$  boson: If  $2m_{\tilde{\tau}_1} < m_{H^0}$ , *i.e.*, if the  $H^0$  boson can go on-shell in the  $b\bar{b}$  and  $gg$  channels, there is the possibility to see the resonance of the  $H^0$  boson in the invariant mass distribution of the staus at  $m_{\tilde{\tau}_1\tilde{\tau}_1^*} \simeq m_{H^0}$  with a width given by  $\Gamma_{H^0}$ .

To illustrate this procedure, we consider four benchmark points,  $\alpha$ ,  $\beta$ ,  $\gamma$ , and  $\epsilon$  within the framework of the CMSSM with parameters listed in table 1. The low-energy SUSY spectrum is obtained using **SPheno** 3.0 [132], while the Higgs sector is recalculated with

Benchmark point		$\alpha$	$\beta$	$\gamma$	$\epsilon$
$m_{1/2}$	[GeV]	600	1050	600	440
$m_0$	[GeV]	800	30	600	20
$\tan \beta$		55	55	55	15
$A_0$	[GeV]	1600	60	1200	−250
$m_{\tilde{\tau}_1}$	[GeV]	193	136	148	153
$\theta_{\tilde{\tau}}$		$81^\circ$	$73^\circ$	$77^\circ$	$76^\circ$
$m_{H^0}$	[GeV]	402	763	413	613
$\Gamma_{H^0}$	[GeV]	15	26	16	2.2
$m_{\tilde{g}}$	[GeV]	1397	2276	1385	1028
avg. $m_{\tilde{q}}$	[GeV]	1370	1943	1287	894
$\mu$	[GeV]	667	1166	648	562
$A_\tau$	[GeV]	515	−143	351	−275
$\text{BR}(b \rightarrow s\gamma)$	$[10^{-4}]$	3.08	3.03	2.94	3.00
$\text{BR}(B_s^0 \rightarrow \mu^+\mu^-)$	$[10^{-8}]$	1.65	1.04	2.44	0.30
$a_\mu$	$[10^{-10}]$	13.2	11.5	16.8	18.7
CCB [107]		✓	—	✓	✓
$Y_{\tilde{\tau}_1}$	$[10^{-15}]$	3.5	2.5	37.7	164

**Table 1:** Benchmark CMSSM scenarios  $\alpha$ ,  $\beta$ ,  $\gamma$ , and  $\epsilon$  defined by the given values of  $m_{1/2}$ ,  $m_0$ ,  $\tan \beta$ , and  $A_0$ . For all points,  $\mu > 0$ . Low-scale masses and parameters are calculated using **SPheno 3.0**. We also provide the quantities that are subject to the constraints discussed in section 2, as obtained with **SuperISO 3.0**, and the thermal relic stau yield  $Y_{\tilde{\tau}_1}$ , as obtained with **micrOMEGAs 2.4**. The CCB constraint (2.10), as obtained in [107], is respected by the scenarios  $\alpha$ ,  $\gamma$ , and  $\epsilon$ , whereas point  $\beta$  is in tension with this constraint.

**FeynHiggs 2.7.4** [116]. We also refer to the constraints discussed in section 2, evaluated with **SuperISO 3.0** [133], and provide the thermal relic stau yield  $Y_{\tilde{\tau}_1}$  as calculated with **micrOMEGAs 2.4** [99]. Benchmark points  $\alpha$  and  $\beta$  are similar to points  $B$  and  $C$  of ref. [74], respectively, where we have adjusted  $m_0$  for point  $\alpha$  and  $m_{1/2}$  for point  $\beta$  so that **SPheno 3.0** provides low-energy spectra that are similar to the ones of those points  $B$  and  $C$ . Point  $\gamma$  is very similar to point  $\alpha$  but has a much larger stau yield. Point  $\epsilon$  was already introduced in ref. [128]. Here, we are mainly interested in the ratio of  $m_{\tilde{\tau}_1}$  and  $m_{H^0}$ . In all four benchmark scenarios, stau production via an on-shell  $H^0$  exchange is possible. We have  $2m_{\tilde{\tau}_1} \approx m_{H^0}$  for point  $\alpha$ ,  $2m_{\tilde{\tau}_1} < m_{H^0}$  for point  $\gamma$ , and  $2m_{\tilde{\tau}_1} \ll m_{H^0}$  for points  $\beta$  and  $\epsilon$ . The stau-Higgs couplings are smallest for point  $\epsilon$ , where  $\tan \beta$  is relatively small.

In figure 8 we display the invariant mass distributions for the four benchmark points at the LHC with  $\sqrt{S} = 14$  TeV. The kinematical cuts (4.1) are applied, with the requirement  $|\eta| < 2.4$  for both staus. The invariant mass distributions show a resonance peak at the mass of the  $H^0$  boson on top of the Drell–Yan continuum in all four considered scenarios. For point  $\alpha$  considered in figure 8(a), the peak is close to the threshold,  $m_{\tilde{\tau}_1\tilde{\tau}_1^*} \approx 2m_{\tilde{\tau}_1}$ , and the distribution falls off steadily at higher invariant masses. Such a Higgs resonance at the beginning of the invariant mass distribution is a strong hint towards efficient stau

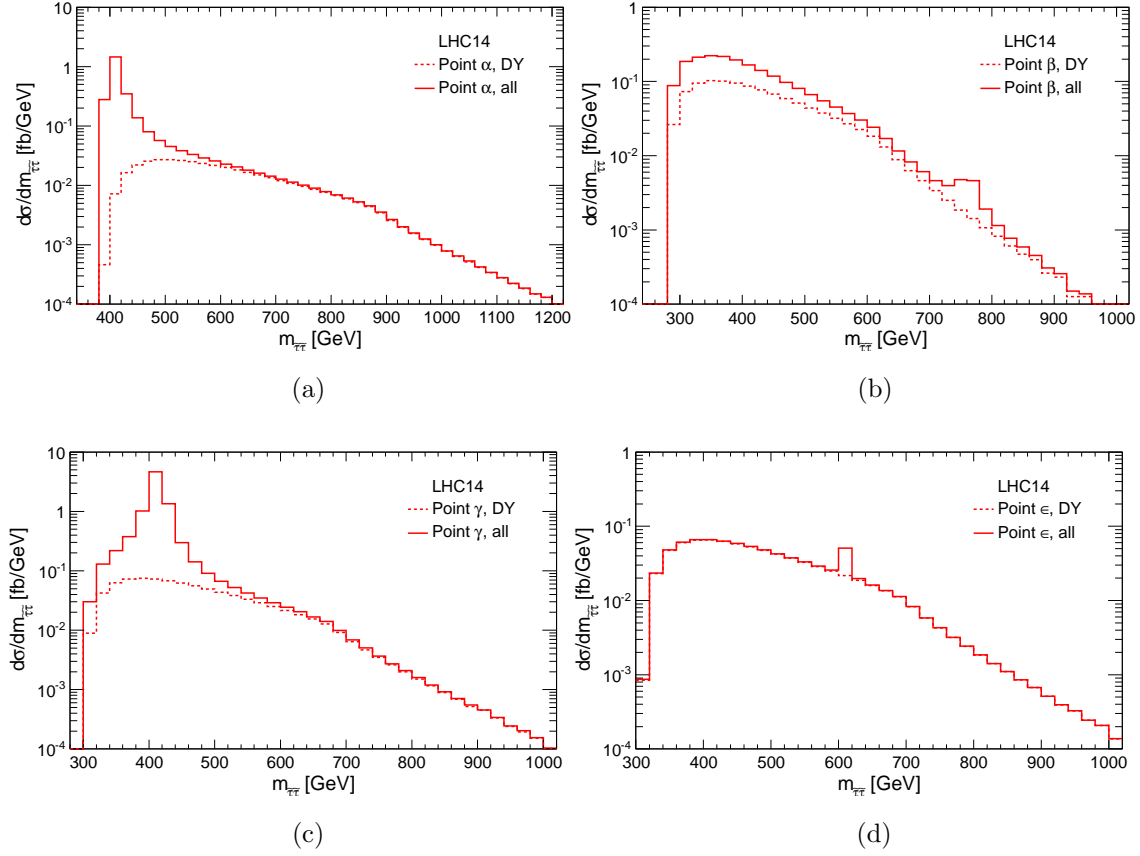


**Figure 8:** Invariant mass distributions of directly produced  $\tilde{\tau}_1 \tilde{\tau}_1^*$  pairs at the LHC with  $\sqrt{S} = 14$  TeV. Drell-Yan predictions are shown by the dashed lines and the full cross sections, including the  $b\bar{b}$  and  $gg$  channels, by the solid lines. The distributions are shown for the benchmark points (a)  $\alpha$ , (b)  $\beta$ , (c)  $\gamma$ , and (d)  $\epsilon$ , which are defined in table 2.

annihilation in the early Universe, as further discussed in section 6 below. In the invariant mass distribution for point  $\gamma$  shown in figure 8(c), the  $H^0$  resonance lies on top of the maximum of the Drell-Yan contribution and the peak is very pronounced. For points  $\beta$  and  $\epsilon$ , the Drell-Yan continuum is dominant and the resonance appears as a small bump at the tail of the distribution as can be seen in figures 8(b) and (d). Note that although the  $b\bar{b}$  and  $gg$  channels do not distort much the shape of the Drell-Yan curve in scenario  $\beta$ , they increase the differential cross section sizeably. This typically happens for large left-right mixing and large  $\tan\beta$  even in the case of an heavy decoupled  $H^0$  boson, see figure 4.

Both the  $\alpha$  and  $\gamma$  scenarios would allow for a determination of the mass  $m_{H^0}$  and also the width  $\Gamma_{H^0}$  (especially in case of point  $\gamma$ ) with a few  $\text{fb}^{-1}$  of data at the LHC with  $\sqrt{S} = 14$  TeV. Nevertheless, also in scenarios with a rather heavy  $H^0$  boson (such as point  $\beta$ ) and in scenarios with small  $\tan\beta$  (such as point  $\epsilon$ ), the LHC might eventually be able to determine the mass  $m_{H^0}$  from the invariant mass distribution of the directly produced long-lived  $\tilde{\tau}_1 \tilde{\tau}_1^*$  pairs. Such a procedure only requires  $2m_{\tilde{\tau}_1} < m_{H^0}$  and is thus generic in large parts of the MSSM parameter space and within the CMSSM. Here a

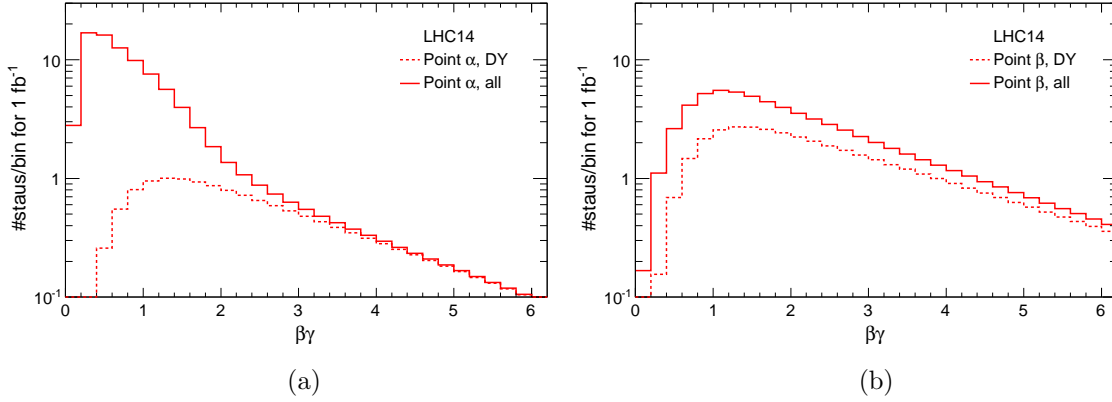


**Figure 9:** Directly produced staus as a function of  $\beta\gamma = |\mathbf{p}|/m$  at the LHC with  $\sqrt{S} = 14$  TeV for an integrated luminosity of  $L = 1 \text{ fb}^{-1}$ . The full results, including  $b\bar{b}$  and  $gg$  channels, are shown by the solid lines and the Drell–Yan predictions by the dashed lines. Staus with  $\beta\gamma \lesssim 0.45$  are expected to get stopped in the LHC detectors. Distributions are shown for the benchmark points (a)  $\alpha$  and (b)  $\beta$ , which are defined in table 1.

future study of theoretical and experimental uncertainties including detector effects and the possible contamination with SUSY backgrounds from cascade decays is necessary to allow for more precise predictions.

### 4.3 Prospects for the stopping of staus

Very slow moving CHAMPs might loose all their momentum and get stopped within the main detector or in some additional stopping detector. The analysis of their subsequent decays may then help to identify the LSP in an R-parity conserving setting (*cf.* section 2.1) or to probe the size of the R-parity violating coupling. In such a way, *e.g.*, the gravitino or axino mass and also its couplings might be tested in the future. In general, as a rule of thumb, CHAMPs with  $\beta\gamma < 0.45$ , as stated in (2.3), are expected to get stopped in the detectors at the LHC. In the following, we show that staus produced directly via the  $b\bar{b}$  and  $gg$  channels provide a large additional source of potentially stopped objects, especially in the cosmologically motivated scenarios discussed in section 2.3.

In figure 9 we give the number of directly produced staus for an integrated luminosity of  $L = 1 \text{ fb}^{-1}$  at the LHC with  $\sqrt{S} = 14$  TeV as a function of  $\beta\gamma = |\mathbf{p}|/m$  for the benchmark points  $\alpha$  and  $\beta$  introduced above and defined in table 1. We only require the pseudo-rapidity of a stau to fulfill  $|\eta| < 2.4$  to be included in the shown histograms. No other kinematical cuts are imposed as we are especially interested in very slow moving objects. We count each produced stau individually.

In both scenarios  $\alpha$  and  $\beta$ , the number of potentially stopped staus, *i.e.*, those with  $\beta\gamma < 0.45$ , is enlarged when the  $b\bar{b}$  and  $gg$  channels are included in the cross section prediction. This enhancement is particularly substantial in scenario  $\alpha$  where  $2m_{\tilde{\tau}_1} \approx m_{H^0}$  and where the staus at the  $H^0$  boson resonance are thus produced almost at rest in the center of mass frame. Here, a large sample of stopped staus could be collected already with



a rather small integrated luminosity. For an integrated luminosity of  $L = 1 \text{ fb}^{-1}$ , about  $N \approx 25$  staus would be stopped, which is encouraging. Indeed, from the Drell–Yan process alone, one would expect only  $N \lesssim 1$ . For an account of the experimental prospects, it is thus crucial to consider also the  $b\bar{b}$  and  $gg$  channels.

## 5. Direct stau production within the CMSSM

In this section we investigate the direct pair production cross section of light staus within the CMSSM. Our aim is to provide a precise prediction for the  $\tilde{\tau}_1 \tilde{\tau}_1^*$  cross section, taking the Drell–Yan process as well as the  $b\bar{b}$  annihilation and  $gg$  fusion channels into account. We are interested in parameter regions with a quasi-stable  $\tilde{\tau}_1$  LOSP, where the  $\tilde{\tau}_1 \tilde{\tau}_1^*$  cross section is of particular importance. We consider the  $m_0$ - $m_{1/2}$  plane of the CMSSM with  $A_0 = 2m_0$ ,  $\tan\beta = 55$ , and  $\mu > 0$ , which is cosmologically motivated by the possible occurrence of exceptional small stau yields [74]. In this plane,  $\tan\beta$  is large and the  $\tilde{\tau}_1$  prefers to be right-handed, *i.e.*,  $\theta_{\tilde{\tau}} > \pi/4$ ; this is generic in the CMSSM due to the different running of the left-handed and right-handed soft masses. Thus, the  $b\bar{b}$  and  $gg$  channels can give large contributions to the stau production cross section. For the CMSSM benchmark scenarios introduced in section 4, we compare our results for direct stau production with indirect stau production mechanisms via the production and decay of other heavier SUSY particles. We find that direct stau production is often the dominant source of staus at colliders, in particular, at lower center-of-mass energies when the production of other SUSY particles is suppressed by their heavier masses.

### 5.1 CMSSM scans of the direct stau pair production cross section

In figures 10 and 11 we show in a  $m_0$ - $m_{1/2}$  plane of the CMSSM the direct stau production cross section at the LHC and at the Tevatron, as well as mass contours and excluded/disfavored parameter regions. For  $A_0 = 2m_0$ ,  $\tan\beta = 55$  and  $\mu > 0$ , we consider the region in which the  $\tilde{\tau}_1$  is the LOSP. Again, we compute the low-energy SUSY spectrum with **SPheno 3.0**, while the Higgs sector is reevaluated with **FeynHiggs 2.7.4**. Flavor constraints are evaluated using **SuperISO 3.0**. The cross section prediction includes the Drell–Yan channels with NLO  $K$ -factors, the  $b\bar{b}$  annihilation and  $gg$  fusion contributions, and the cuts (4.1) adequate for a long-lived stau are applied. The white area in the lower left is excluded by a tachyonic spectrum, impossible electroweak symmetry breaking (EWSB), or a stau mass  $m_{\tilde{\tau}_1} \leq 82 \text{ GeV}$  below the conservative LEP limit (2.1). In the upper left white area, the LOSP is the lightest neutralino  $\tilde{\chi}_1^0$  (as indicated). In the gray area around  $m_0 \sim m_{1/2} \sim 500 \text{ GeV}$ ,  $\text{BR}(B_s^0 \rightarrow \mu^+ \mu^-)$  exceeds the upper limit given in (2.11). The hatched area is disfavored by the CCB constraint (2.10). Contours for a constant Higgs mass of  $m_{h^0} = 113 \text{ GeV}$  and  $114 \text{ GeV}$  are shown as thin solid black lines. The dashed black lines are  $m_{\tilde{\tau}_1}$  contours and the solid white lines  $m_{H^0}$  contours, where the associated mass values are indicated on the respective contours in units of GeV.

The cross section depends mainly on  $m_{\tilde{\tau}_1}$  and  $m_{H^0}$  and varies over several orders of magnitude in the given parameter ranges. At the LHC with  $\sqrt{S} = 14 \text{ TeV}$ , it reaches  $10^3 \text{ fb}$  in the region with  $m_0 \lesssim 700 \text{ GeV}$  and  $m_{1/2} \lesssim 500 \text{ GeV}$  and drops to  $\lesssim 2 \times 10^{-2} \text{ fb}$

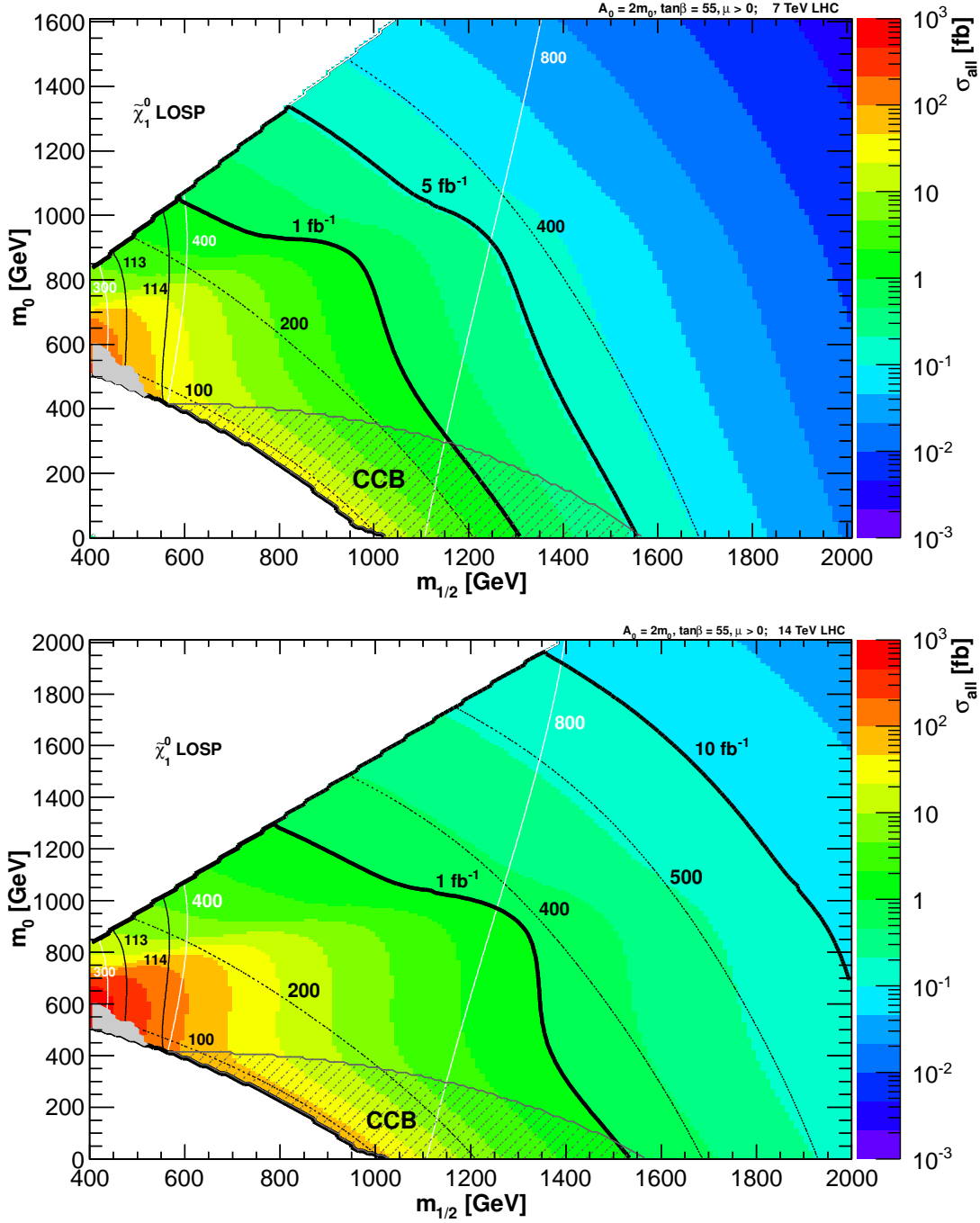


**Figure 10:** Contours of the total direct  $\tilde{\tau}_1 \tilde{\tau}_1^*$  production cross section (shaded, colored) at the LHC with  $\sqrt{S} = 7$  TeV (top) and 14 TeV (bottom) after the cuts (4.1) in the CMSSM  $m_0$ - $m_{1/2}$  plane with  $\tan \beta = 55$ ,  $A_0 = 2m_0$ , and  $\mu > 0$ . The white region in the lower left is excluded because of a tachyonic spectrum, impossible EWSB, or  $m_{\tilde{\tau}_1} \leq 82$  GeV. In the upper white area, the lightest neutralino  $\tilde{\chi}_1^0$  is the LOSP. Parameter points in the gray area around  $m_0 \sim m_{1/2} \sim 500$  GeV do not respect the constraint  $\text{BR}(B_s^0 \rightarrow \mu^+ \mu^-) < 4.3 \times 10^{-8}$ . The lower hatched area is in tension with the CCB constraint (2.10). The thin solid black lines indicate  $m_{h^0}$ , the dashed black lines  $m_{\tilde{\tau}_1}$ , and the white lines  $m_{H^0}$ , where the mass values are given in units of GeV at the respective contour. For a naive estimate of the discovery potential, thick black lines show regions in which at least one  $\tilde{\tau}_1 \tilde{\tau}_1^*$ -pair-production event is expected for integrated luminosities of  $\mathcal{L} = 1 \text{ fb}^{-1}$  and  $5 \text{ fb}^{-1}$  at  $\sqrt{S} = 7$  TeV and  $\mathcal{L} = 1 \text{ fb}^{-1}$  and  $10 \text{ fb}^{-1}$  at  $\sqrt{S} = 14$  TeV.

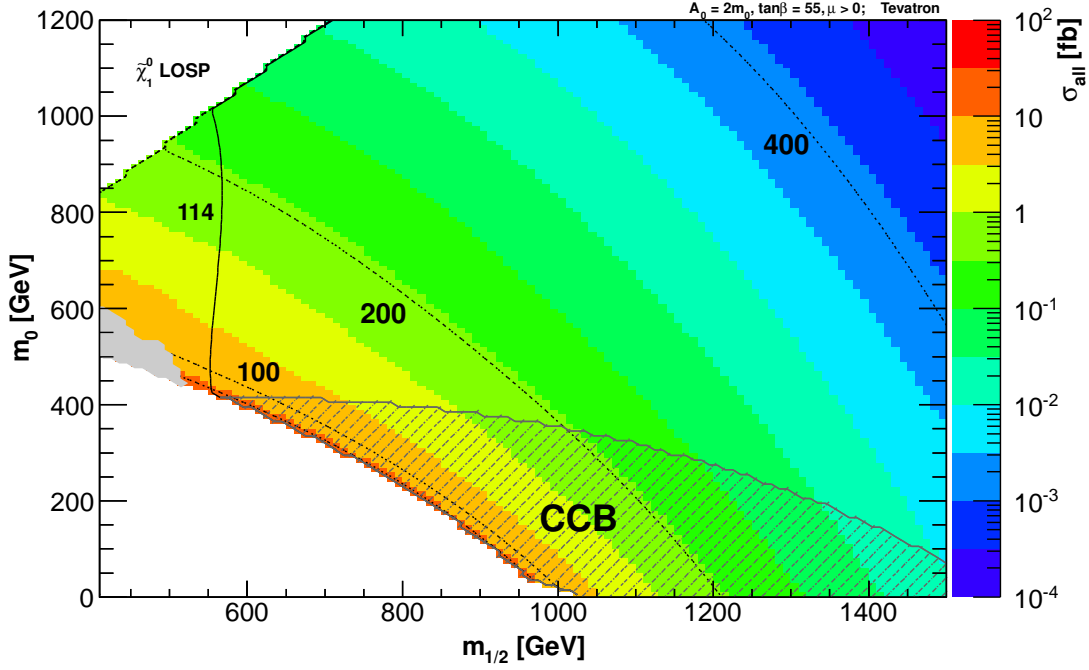


**Figure 11:** Contours of the total direct  $\tilde{\tau}_1 \tilde{\tau}_1^*$  production cross section (shaded, colored) at the Tevatron with  $\sqrt{S} = 1.96$  TeV after the cuts (4.1) in the CMSSM  $m_0$ - $m_{1/2}$  plane with  $\tan\beta = 55$ ,  $A_0 = 2m_0$ , and  $\mu > 0$ . All shown contours and regions are as in figure 10. A tiny (dark orange) strip with  $\sigma > 10$  fb is in tension with searches for CHAMPs at the Tevatron [97].

for, *e.g.*,  $m_0 \sim m_{1/2} \sim 2$  TeV, as can be seen in the lower panel of figure 10. When going down from  $\sqrt{S} = 14$  TeV to 7 TeV, considered in the upper panel of figure 10, we observe a decrease of the cross section by up to about a factor of 5 (see also figures 5 and 6). To give a naive estimate of the discovery potential, we also show contours (thick lines) on which one  $\tilde{\tau}_1 \tilde{\tau}_1^*$ -pair-production event is expected for integrated luminosities of  $\mathcal{L} = 1 \text{ fb}^{-1}$  and  $5 \text{ fb}^{-1}$  at  $\sqrt{S} = 7$  TeV and  $\mathcal{L} = 1 \text{ fb}^{-1}$  and  $10 \text{ fb}^{-1}$  at  $\sqrt{S} = 14$  TeV. The parameter regions to the left of these lines could thus be accessible by the experiments at the LHC already in the very near future, in particular, since the SM backgrounds are expected to be well under control with the kinematical cuts discussed above. However, a more realistic determination of the discovery reach and/or the exclusion limits should be performed in the context of a detailed study including detector effects. Such a study has been performed recently in the case of direct Drell–Yan production [131].

At the Tevatron, the overall cross section for the direct production of staus is much smaller than at the LHC. As can be seen from figure 11, it ranges typically from some tenths to a few femtobarns. (Here we should note that the shading/color scales in figure 11 differ from the ones in figure 10). Larger values in the considered CMSSM plane are only found very close to the region excluded by the LEP mass limit (2.1) in the lower left corner of figure 11. Here, in a tiny strip of the parameter plane, the cross section exceeds  $10 \text{ fb}$  (as indicated by the dark orange color coding) and thus challenges the current cross section limit (2.2) from the CDF experiment [97].

The actual shape of the cross section and mass contours in the  $m_0$ - $m_{1/2}$  planes can easily be understood. We focus here on parameter regions with a  $\tilde{\tau}_1$  LOSP, where typically  $m_{1/2} > m_0$  in the CMSSM. For  $\tan \beta > 20$ , the  $A^0$  mass can approximately be written as  $m_A^2 \approx m_0^2 + 2.5m_{1/2}^2$  (neglecting Yukawa interactions) [134] and thus  $m_A$  is mainly determined by  $m_{1/2}$ . For  $m_{1/2} \gg 0$ , the Higgs sector is then typically in the decoupling limit, where  $m_{H^0} \approx m_A$ , and thus  $m_{H^0}$  also mainly determined by  $m_{1/2}$ . The dependence of  $m_{\tilde{\tau}_1}$  on  $m_0$  and  $m_{1/2}$  is less intuitive in the discussed parameter range ( $\tilde{\tau}_1$  LOSP, large  $\tan \beta$ , sizeable Yukawa couplings), but the usual relation  $m_{\tilde{\tau}_1}^2 \propto m_0^2 + 0.15m_{1/2}^2$  [134] can still be considered. Thus, one finds for  $m_{1/2} \gg m_0$  that it is always  $m_{H^0} > 2m_{\tilde{\tau}_1}$ . For the stau production cross section, this means that there can be important contributions from the  $b\bar{b}$  and  $gg$  channels in the region  $m_{1/2} \gg m_0$ , where the  $H^0$  boson can go on-shell. Towards large  $m_0$  and  $m_{1/2}$ , however, the  $\tilde{\tau}_1$  and (even faster) the  $H^0$  become heavy and contributions from the  $b\bar{b}$  and  $gg$  channels become less important compared to the Drell–Yan channel. If the Drell–Yan contributions dominate, the overall production cross section is basically a function of the  $\tilde{\tau}_1$  mass and decreases strongly for higher  $m_{\tilde{\tau}_1}$ .

Close to the boundary of the  $\tilde{\chi}_1^0$  LOSP region, where  $m_0 \approx m_{1/2}$ , the  $\tilde{\tau}_1$  gets heavier relative to the  $H^0$  boson so that  $2m_{\tilde{\tau}_1} > m_{H^0}$ , which means that the direct stau production via an on-shell  $H^0$  boson is no longer possible. However, the position of the transition at  $2m_{\tilde{\tau}_1} = m_{H^0}$  depends strongly on  $\tan \beta$ . For large  $\tan \beta$ , bottom and tau Yukawa couplings can be sizable and drive down the masses of the heavy Higgses. For small  $\tan \beta$ , this transition lies mostly within the  $\tilde{\chi}_1^0$  LOSP region and only for very large values of  $m_{1/2}$  within the  $\tilde{\tau}_1$  LOSP region. Thus, for smaller values of  $\tan \beta$ , contributions from on-shell  $H^0$  boson exchange are a generic feature of the CMSSM, as one usually finds  $2m_{\tilde{\tau}_1} < m_{H^0}$ .

Let us emphasize that even if the  $b\bar{b}$  and  $gg$  contributions are not necessarily large in parameter regions with  $m_{H^0} > 2m_{\tilde{\tau}_1}$ , *i.e.*, when the  $H^0$  boson is heavy, this configuration still opens the channels for stau production via on-shell  $H^0$  exchange. As discussed in section 4.2, this could allow us to determine the  $H^0$  boson width and mass by investigating the  $\tilde{\tau}_1 \tilde{\tau}_1^*$  invariant mass distribution.

## 5.2 Direct stau production vs. staus from cascade decays

So far we have focused on the analysis of direct stau production. But in a  $\tilde{\tau}_1$  LOSP scenario, staus will also be generated in any SUSY particle production process where heavier sparticles are produced that cascade down to lighter ones and eventually decay into the LOSP, with SM particles emitted along the SUSY decay chain. At hadron colliders, the largest contribution to the overall SUSY cross section is usually expected to originate from the production and subsequent decay of color-charged SUSY particles, *i.e.*, squarks and gluinos. However, also direct production of neutralinos and charginos (*e.g.*,  $\tilde{\chi}_i^0 \tilde{\chi}_j^\pm$ ) and associated production of a neutralino or chargino with a gluino or squark can give sizeable contributions in large parts of the allowed SUSY parameter space.

In table 2 we compare our predictions for the direct  $\tilde{\tau}_1 \tilde{\tau}_1^*$ -pair production cross sections contributions from the Drell–Yan,  $b\bar{b}$  annihilation, and  $gg$  fusion channels with the inclusive cross section for other SUSY particle production cross sections, calculated at NLO with **Prospino 2**, for the benchmark points defined in table 1. (Note that an average squark mass  $m_{\tilde{q}}$  is listed in table 1.) We sum over all possible combinations of squark, neutralino, and chargino eigenstates. For simplicity, we consider inclusive cross sections without any kinematical cuts. Only for the direct stau production channels, cross sections after applying the cuts (4.1) are additionally given in parentheses. Considering the LHC, each cross section is listed for  $\sqrt{S} = 7$  TeV and 14 TeV.

From a comparison of the inclusive production cross sections, we can see that direct stau production is an important source of staus for the benchmark points  $\alpha$ ,  $\beta$ , and  $\gamma$  at the LHC with  $\sqrt{S} = 7$  TeV. Only electroweak neutralino/chargino pair production ( $\tilde{\chi}\tilde{\chi}$ ) can give comparable contributions. We even find that direct stau production can constitute the dominant part of the overall SUSY cross section together with  $\tilde{\chi}\tilde{\chi}$  production. The other cross sections are suppressed at  $\sqrt{S} = 7$  TeV by the heavier masses of squarks and gluinos. The situation changes for  $\sqrt{S} = 14$  TeV, where the center-of-mass energy is high enough so that strongly interacting SUSY particles can be produced copiously. However, for point  $\beta$ , where  $m_{1/2}$  is particularly large, the gluino is so heavy that direct stau production is always the dominant source for staus at colliders. Still, we annotate that the LHC at  $\sqrt{S} = 7$  TeV might in some scenarios provide a more suitable environment for the study of direct stau production than the LHC at  $\sqrt{S} = 14$  TeV, where staus originating from cascade decays would need to be suppressed by additional cuts.

It is also interesting to look more closely at the composition of the total direct stau production cross section in these scenarios. Points  $\alpha$  and  $\gamma$  have a very similar composition of  $\sigma(\tilde{\tau}_1 \tilde{\tau}_1^*)_{\text{all}}$  (but a very different stau yield, see also section 6) and the  $b\bar{b}$  annihilation channel is the dominant stau production mechanism for both points.

Benchmark point		$\alpha$	$\beta$	$\gamma$	$\epsilon$
LHC 7 TeV					
$\sigma(\tilde{\tau}_1 \tilde{\tau}_1^*)_{\text{DY}}$	[fb]	3.2(2.3)	12.5 (7.3)	9.0 (5.6)	7.95 (5.00)
$\sigma(\tilde{\tau}_1 \tilde{\tau}_1^*)_{b\bar{b}}$	[fb]	9.8 (5.1)	0.03 (0.02)	19.2 (16.5)	0.07 (0.06)
$\sigma(\tilde{\tau}_1 \tilde{\tau}_1^*)_{gg}$	[fb]	0.1 (0.1)	3.3 (2.4)	0.32 (0.25)	0.01 (0.01)
$\sigma(\tilde{\tau}_1 \tilde{\tau}_1^*)_{\text{all}}$	[fb]	13.1 (7.5)	15.8 (9.7)	28.5 (22.4)	8.03 (5.07)
$\sigma(\tilde{g}\tilde{g})$	[fb]	0.05	$10^{-6}$	0.06	2.57
$\sigma(\tilde{g}\tilde{q})$	[fb]	0.63	$4 \times 10^{-4}$	0.99	37.36
$\sigma(\tilde{q}\tilde{q})$	[fb]	1.18	0.006	2.41	77.25
$\sigma(\tilde{\chi}\tilde{q}) + \sigma(\tilde{\chi}\tilde{g})$	[fb]	0.481	0.007	0.72	12.77
$\sigma(\tilde{\chi}\tilde{\chi})$	[fb]	20.4	0.29	19.8	91.78
LHC 14 TeV					
$\sigma(\tilde{\tau}_1 \tilde{\tau}_1^*)_{\text{DY}}$	[fb]	11.2 (5.64)	37.5 (15.9)	28.0 (12.4)	24.7 (11.2)
$\sigma(\tilde{\tau}_1 \tilde{\tau}_1^*)_{b\bar{b}}$	[fb]	58.4 (27.0)	0.7 (0.2)	113.3 (87.1)	0.5 (0.4)
$\sigma(\tilde{\tau}_1 \tilde{\tau}_1^*)_{gg}$	[fb]	0.7 (0.4)	17.4 (11.1)	1.8 (1.3)	0.07 (0.05)
$\sigma(\tilde{\tau}_1 \tilde{\tau}_1^*)_{\text{all}}$	[fb]	70.3 (33.1)	55.6 (27.2)	143.1 (100.8)	25.3 (11.6)
$\sigma(\tilde{g}\tilde{g})$	[fb]	20.2	0.12	20.8	232.19
$\sigma(\tilde{g}\tilde{q})$	[fb]	104.4	2.46	133.2	1328.4
$\sigma(\tilde{q}\tilde{q})$	[fb]	92.5	6.46	139.0	1301.1
$\sigma(\tilde{\chi}\tilde{q}) + \sigma(\tilde{\chi}\tilde{g})$	[fb]	16.9	1.08	22.4	175.12
$\sigma(\tilde{\chi}\tilde{\chi})$	[fb]	134.5	6.40	131.1	422.2

**Table 2:** Hadronic cross sections for various SUSY pair production processes at the LHC with  $\sqrt{S} = 7$  TeV and 14 TeV. For direct  $\tilde{\tau}_1 \tilde{\tau}_1^*$ -pair production, we list our cross section results before and after applying the kinematical cuts (4.1), where the latter are given in parantheses. The other cross sections are inclusive NLO results obtained with **Prospino** 2, where no kinematical cuts have been considered.

Benchmark point  $\beta$  is considered to illustrate the impact of a large  $\tilde{\tau}_1 \tilde{\tau}_1^* h^0$  coupling. Here, large values of  $\mu$  and  $\tan\beta$  together with a relatively large mixing result in this large coupling (*cf.* section 2.3 and appendix A.2). However, such very large couplings are in strong conflict with CCB constraint (2.10). For this point, the  $H^0$  boson is very massive and  $b\bar{b}$  annihilation and gluon fusion into an intermediate  $H^0$  boson is suppressed by the heavy particle’s propagator. Stau production is thereby dominated by the Drell–Yan channel and gets sizeable contributions from the gluon fusion channel, where especially processes mediated by the  $h^0$  boson are important.

Finally, benchmark scenario  $\epsilon$  differs from the above scenarios by much smaller values of  $m_{1/2}$  and  $\tan\beta$ . It could be considered a ‘typical’  $\tilde{\tau}_1$  LOSP scenario, without an exceptional stau yield. In this case, the direct stau production cross section is well described by the Drell–Yan process, whereas the  $b\bar{b}$  and  $gg$  channels are basically negligible. Moreover, the indirect stau production mechanisms are much more efficient than the direct ones.

## 6. Collider tests of an exceptionally small relic stau abundance

In the preceding sections we have considered various aspects of stau production at hadron colliders with emphasis on parameter regions that allow for an exceptionally small yield of a long-lived stau (2.8). Because of the appealing features described in section 2.3, we now discuss the testability of such an exceptional yield in collider experiments. While related prospects for collider phenomenology were already addressed in refs. [73, 74, 106, 110], we show here for the first time that contributions from  $b\bar{b}$  annihilation and gluon fusion to direct stau production can play a particularly important role for this testability at hadron colliders.

Assuming a standard cosmological history with a reheating temperature  $T_R > m_{\tilde{\tau}_1}/20$ , the key requirements for an exceptionally small thermal relic stau yield (2.8) are (i) a relatively small stau mass of  $m_{\tilde{\tau}_1} \lesssim 200$  GeV, (ii) the mass pattern  $2m_{\tilde{\tau}_1} \simeq m_{H^0}$ , which allows for primordial  $\tilde{\tau}_1$  annihilation via the  $H^0$  resonance [74], and/or (iii) enhanced stau-Higgs couplings, which are often associated with a sizeable stau-left-right mixing [73, 74], as described in section 2.3 and appendix A.2. Now, our studies of direct stau production in the previous sections demonstrate clearly that the contributions from  $b\bar{b}$  annihilation and gluon fusion are sensitive to all three of these requirements. In contrast, the Drell–Yan process is sensitive to  $m_{\tilde{\tau}_1}$  and the stau-mixing angle  $\theta_{\tilde{\tau}}$  only.

### Excess of direct stau production cross sections over Drell–Yan predictions

Based on our results in sections 3.2 and 5, we already know that  $b\bar{b}$ -annihilation and gluon-fusion processes can lead to direct stau production cross sections that exceed the Drell–Yan predictions significantly, in particular, for  $2m_{\tilde{\tau}_1} \lesssim m_{H^0}$  and/or enhanced stau-Higgs couplings. This motivates us to explore the ratio

$$R = \sigma(\tilde{\tau}_1 \tilde{\tau}_1^*)_{\text{all}} / \sigma(\tilde{\tau}_1 \tilde{\tau}_1^*)_{\text{DY}} \quad (6.1)$$

as a potential indicator for a cosmological scenario with an exceptionally small stau yield. Here the total direct stau production cross section,  $\sigma(\tilde{\tau}_1 \tilde{\tau}_1^*)_{\text{all}}$ , and the Drell–Yan prediction,  $\sigma(\tilde{\tau}_1 \tilde{\tau}_1^*)_{\text{DY}}$ , are considered after applying the cuts (4.1) for scenarios with a long-lived stau.

Before presenting and discussing our theoretical results for  $R$ , let us comment on its experimental determination which will have to rely on measurements of  $m_{\tilde{\tau}_1}$  and  $\sigma(\tilde{\tau}_1 \tilde{\tau}_1^*)_{\text{all}}$ . While an accuracy of  $< 1\%$  is expected for a  $m_{\tilde{\tau}_1}$  determination at the LHC [23, 26],  $\sigma(\tilde{\tau}_1 \tilde{\tau}_1^*)_{\text{all}}$  measurements may be more difficult, as mentioned in section 4. If indirect stau production is significant, they will require jet/lepton vetos and/or additional kinematical cuts. With a precisely known  $m_{\tilde{\tau}_1}$ ,  $\sigma(\tilde{\tau}_1 \tilde{\tau}_1^*)_{\text{DY}}$  can be calculated theoretically with an uncertainty of about a factor of 2 that is related to its dependence on  $\theta_{\tilde{\tau}}$ ; see figures 3 (b) and 4 (a). To obtain a conservative estimate of  $R$ , one will then evaluate (6.1) with the maximum  $\sigma(\tilde{\tau}_1 \tilde{\tau}_1^*)_{\text{DY}}$  at  $\theta_{\tilde{\tau}} = 0$ . In fact, as already addressed in section 4.2, a measurement of  $\theta_{\tilde{\tau}}$  based on direct stau production is conceivable only if the Drell–Yan contribution dominates, *i.e.*, for  $R \simeq 1$ . On the other hand, studies of staus produced in cascade decays may help to indirectly probe  $\theta_{\tilde{\tau}}$  [36] and thereby to determine  $R$  more precisely. Thus, we present in the following results for  $R$  that are not conservative estimates but theoretical

Benchmark point	$\alpha$	$\beta$	$\gamma$	$\epsilon$
$R_{\text{LHC7}}$	3.3	1.3	4.0	1.01
$R_{\text{LHC14}}$	5.8	1.7	8.1	1.04
$Y_{\tilde{\tau}_1} [10^{-15}]$	3.5	2.5	37.7	164

**Table 3:** The stau yield  $Y_{\tilde{\tau}_1}$  and  $R = \sigma(\tilde{\tau}_1\tilde{\tau}_1^*)_{\text{all}}/\sigma(\tilde{\tau}_1\tilde{\tau}_1^*)_{\text{DY}}$  at the LHC with  $\sqrt{S} = 7$  TeV ( $R_{\text{LHC7}}$ ) and 14 TeV ( $R_{\text{LHC14}}$ ) for the benchmark scenarios  $\alpha$ ,  $\beta$ ,  $\gamma$  and  $\epsilon$ , defined in table 1 and partially indicated in figure 12. The stau yield is obtained from `micrOMEGAs 2.4` and the  $R$  values from the respective cross sections after kinematical cuts (4.1) given in parantheses in table 2.

predictions taking into account  $\sigma(\tilde{\tau}_1\tilde{\tau}_1^*)_{\text{DY}}$  with its full  $\theta_{\tilde{\tau}}$  dependence. For an unknown  $\theta_{\tilde{\tau}}$ ,  $R > 2$  will then be a required indication for sizeable contributions of the  $b\bar{b}$  and  $gg$  channels.

In figure 12 the shaded (colored) contours indicate our theoretical predictions for  $R$  at the LHC with  $\sqrt{S} = 7$  TeV (top panel) and 14 TeV (bottom panel) in the  $m_0$ - $m_{1/2}$  CMSSM plane with  $A_0 = 2m_0$ ,  $\tan\beta = 55$ , and  $\mu > 0$ . The white lines show contours of  $Y_{\tilde{\tau}_1} = 4 \times 10^{-15}$ ,  $10^{-14}$ ,  $4 \times 10^{-14}$  as obtained with `micrOMEGAs 2.4` [99]. The labeled (red) stars indicate the location of the benchmark points  $\alpha$ ,  $\beta$ , and  $\gamma$ , defined in table 1. Excluded and unconsidered regions are as in figure 10, and also the region disfavored by the CCB constraint (2.10) is indicated but now by the gray hatched region.

The  $R$  contours show very explicitly that the Drell–Yan prediction can underestimate the direct  $\tilde{\tau}_1\tilde{\tau}_1^*$  production cross section by up to a factor of 10 (20) for  $\sqrt{S} = 7$  TeV (14 TeV). This demonstrates again the potential importance of the  $b\bar{b}$  and  $gg$  channels included in our calculations. In fact, their effect with respect to the Drell–Yan predictions is more relevant at  $\sqrt{S} = 14$  TeV than at 7 TeV. This results from the  $b\bar{b}$  and gluon luminosities in the proton that benefit more strongly from the higher  $\sqrt{S}$  than those of the lighter quarks. On the other hand, also indirect stau production can be much more efficient for  $\sqrt{S} = 14$  TeV; cf. table 2. Thereby, it may even be more difficult to identify direct stau production events at  $\sqrt{S} = 14$  TeV despite potentially larger values of  $R$ .

In table 3 we list the  $R$  values at the LHC with  $\sqrt{S} = 7$  TeV ( $R_{\text{LHC7}}$ ) and 14 TeV ( $R_{\text{LHC14}}$ ) and the stau yield  $Y_{\tilde{\tau}_1}$  for the benchmark points  $\alpha$ ,  $\beta$ ,  $\gamma$ , and  $\epsilon$ . We see again that  $R$  increases when going from  $\sqrt{S} = 7$  TeV to 14 TeV. This effect is most pronounced for the points  $\alpha$  and  $\gamma$  for which  $b\bar{b}$  annihilation dominates the direct stau production cross section. A considerable 30% increase of  $R$  is predicted also for point  $\beta$  for which gluon fusion contributes up to about 40% of  $\sigma(\tilde{\tau}_1\tilde{\tau}_1^*)_{\text{all}}$ ; cf. table 2.

To understand the shape of the  $R$  contours in figure 12, it is instructive to look at the lines of constant  $m_{\tilde{\tau}_1}$  and  $m_{H^0}$ , which are shown for the same CMSSM parameter choice in figure 10. By interpolating between the intersections of the  $m_{\tilde{\tau}_1} = 200$  GeV and  $m_{H^0} = 400$  GeV and of the  $m_{\tilde{\tau}_1} = 400$  GeV and  $m_{H^0} = 800$  GeV contours, one can infer the location of the line with  $2m_{\tilde{\tau}_1} = m_{H^0}$ . Only below this line, on-shell  $H^0$  exchange is possible and can lead to  $R \gg 2$  in the vicinity of this line, where a smaller  $m_{H^0}$  allows for a larger  $R$ . By going along a contour on which  $m_{\tilde{\tau}_1}$  does not change (such as the  $m_{\tilde{\tau}_1} = 200$  GeV contour) from the region with smaller  $m_{H^0}$  into the direction with larger



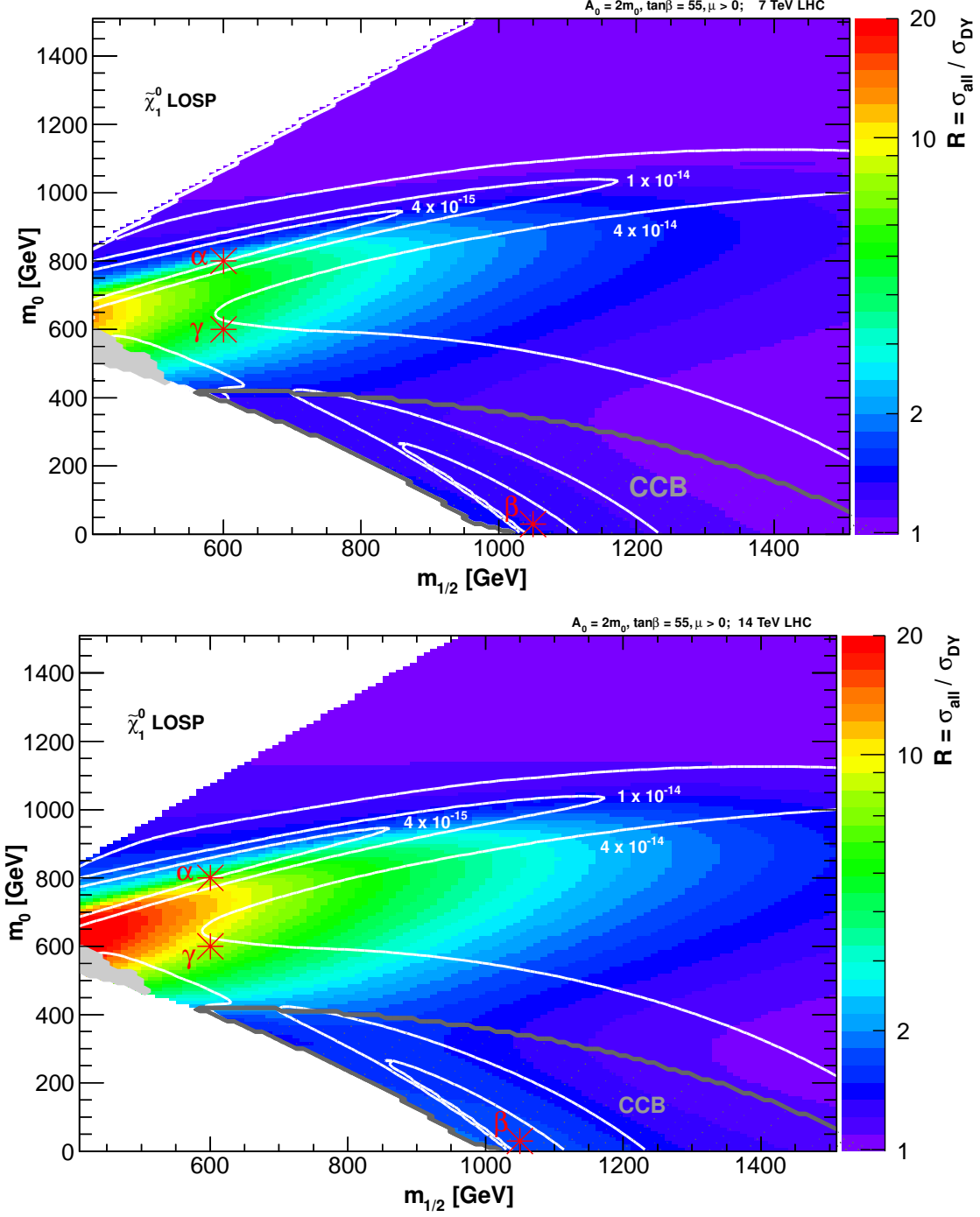


**Figure 12:** The ratio  $R = \sigma(\tilde{\tau}_1 \tilde{\tau}_1^*)_{\text{all}} / \sigma(\tilde{\tau}_1 \tilde{\tau}_1^*)_{\text{DY}}$  (shaded contours, colored) for the LHC with  $\sqrt{S} = 7$  TeV (top panel) and 14 TeV (bottom panel) and  $Y_{\tilde{\tau}_1} = 4 \times 10^{-15}, 10^{-14}, 4 \times 10^{-14}$  (white lines) in the  $m_0$ - $m_{1/2}$  CMSSM plane with  $A_0 = 2m_0$ ,  $\tan\beta = 55$ , and  $\mu > 0$ . The CCB constraint (gray hatched region) and excluded/unconsidered regions are as in figure 10. The labeled (red) stars indicate the location of the benchmark points  $\alpha$ ,  $\beta$ , and  $\gamma$ , defined in table 1.

$m_{H^0}$ , one encounters the qualitative behavior that is illustrated in figure 3 (c).

Let us now turn to the main aspects of the  $Y_{\tilde{\tau}_1}$  contours in figure 12; for additional details we refer to [74] in which those contours were studied in the same CMSSM plane. An exceptionally small yield (2.8) can be found in the two separate regions enclosed by the  $Y_{\tilde{\tau}_1} = 4 \times 10^{-15}$  contour. The region, to which point  $\alpha$  belongs, allows for primordial  $\tilde{\tau}_1$  annihilation via the  $H^0$  resonance, and the region, to which point  $\beta$  belongs, for efficient  $\tilde{\tau}_1$  annihilation via enhanced stau-Higgs couplings. While the latter region is in conflict with the CCB constraint (2.10), we still include this point in our discussion of the testability of an exceptionally small  $Y_{\tilde{\tau}_1}$  at colliders.

Comparing regions with  $R \gtrsim 2$  to those with  $Y_{\tilde{\tau}_1} < 4 \times 10^{-15}$ , we find that there is no one-to-one link between a sizeable  $R$  value and an exceptionally small yield. For example, while the point  $\beta$  is associated with such an exceptional yield, we obtain  $R < 2$ , even at the LHC with  $\sqrt{S} = 14$  TeV, as can be seen in table 3. Moreover, in figure 12, also moderate values of  $R \simeq 2$ –3 occur in the  $2m_{\tilde{\tau}_1} \simeq m_{H^0}$  region enclosed by the  $Y_{\tilde{\tau}_1} < 4 \times 10^{-15}$  contour. On the other hand, point  $\gamma$  is associated with  $R \simeq 4$ –8 while the yield at this point exceeds the limit (2.8) by more than one order of magnitude. Only for points such as  $\alpha$ , one finds both an exceptionally large  $R \simeq 3$ –6 and an exceptionally small stau yield. Thus, a sizeable  $R$  could very well be a first hint for the possibility of efficient stau-annihilation in the early Universe but additional investigations will be crucial to clarify the situation.

### Exceptional $Y_{\tilde{\tau}_1}$ and $R$ in models with non-universal Higgs masses

Before proceeding, we would like to illustrate more clearly that a region with resonant primordial stau annihilation and an exceptionally small  $Y_{\tilde{\tau}_1}$  can be associated with different values of  $R$ . The resonance condition  $2m_{\tilde{\tau}_1} \approx m_{H^0}$  is found in  $m_0$ – $m_{1/2}$  CMSSM planes only in a small horizontal ‘funnel’ region and for specific combinations of parameters. In less constrained models with non-universal Higgs masses (NUHM) this mass pattern occurs in a more generic way and already for smaller values of  $\tan \beta$ .

In figure 13 we consider a scenario in which the two Higgs mass parameters are equal (and negative) but different from the other high scale scalar mass parameter,  $m_{H_u} = m_{H_d} = m_0^H \neq m_0$ , which is a framework denoted as NUHM1 model. We vary  $m_0^H$  and set the other parameters to  $m_0 = 50$  GeV,  $m_{1/2} = 400$  GeV,  $\tan \beta = 30$ ,  $A_0 = 0$ , and  $\mu > 0$ , which are defined as in the CMSSM. In the top panel,  $m_{H^0}$  is indicated by the solid (red) line,  $m_{h^0}$  by the dashed (green) line, and  $m_{\tilde{\tau}_1}$  by the dotted (blue) line. The middle panel shows  $Y_{\tilde{\tau}_1}$ . In the bottom panel,  $\sigma(\tilde{\tau}_1 \tilde{\tau}_1^*)_{\text{DY}}$  is shown by the solid (red) line,  $\sigma(\tilde{\tau}_1 \tilde{\tau}_1^*)_{\text{all}}$  by the dashed (green) line, and  $R$  by the dotted (blue) line. Note that the negative mass parameter  $m_0^H$  has to be understood as the root of the modulus of a negative squared soft-mass of the Higgses. For a more negative  $m_0^H$ , the  $\tilde{\tau}_1$  is no longer the LOSP and eventually (*i.e.*, for an even more negative  $m_0^H$ ) the stability bound  $m_{H_u/d}^2 + |\mu|^2 \geq 0$  can be violated at  $M_{\text{GUT}}$ . In such cases, there might be a vacuum instability leading to electroweak symmetry breaking already at  $M_{\text{GUT}}$ .

Considering the top panel, one sees that  $m_{H^0}$  gets smaller and  $m_{\tilde{\tau}_1}$  larger towards smaller values of  $m_0^H$ . For  $m_0^H \simeq -815$  GeV, one finds the resonance condition  $2m_{\tilde{\tau}_1} = m_{H^0}$ . In a narrow region around this point, a significant depletion of the stau yield  $Y_{\tilde{\tau}_1}$  by

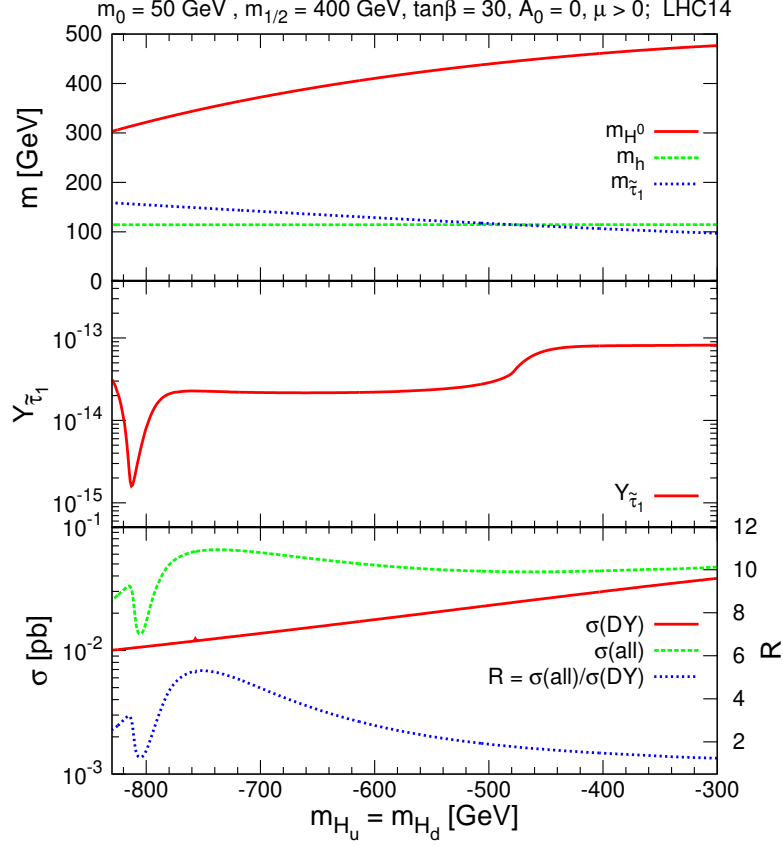


**Figure 13:** The masses  $m_{\tilde{\tau}_1}$ ,  $m_{h^0}$ , and  $m_{H^0}$  (top panel), the stau yield  $Y_{\tilde{\tau}_1}$  (middle panel), the cross sections  $\sigma(\tilde{\tau}_1 \tilde{\tau}_1^*)_{all}$  and  $\sigma(\tilde{\tau}_1 \tilde{\tau}_1^*)_{DY}$  and  $R$  at the LHC with  $\sqrt{S} = 14$  TeV (bottom) as a function of the Higgs-mass parameter  $m_{H_u} = m_{H_d} = m_0^H$ , defined at the high scale, in the NUHM1 model with  $m_{1/2} = 400$  GeV,  $m_0 = 50$ ,  $\tan\beta = 30$ ,  $A_0 = 0$ .

about one order of magnitude down to an exceptional value of  $\lesssim 2 \times 10^{-15}$  can be seen in the middle panel. To the right of this resonance point, *i.e.*, for  $m_0^H > -815$  GeV,  $2m_{\tilde{\tau}_1} < m_{H^0}$  so that on-shell  $H^0$ -boson exchange can contribute to direct stau production. Thereby, this leads to a significant contribution of the  $b\bar{b}$  and  $gg$  channels to  $\sigma(\tilde{\tau}_1 \tilde{\tau}_1^*)_{all}$  and  $R$  increases significantly up to about 5. However, the maximum of  $\sigma(\tilde{\tau}_1 \tilde{\tau}_1^*)_{all}$  and of  $R$  is shifted away from the resonance point at which  $Y_{\tilde{\tau}_1}$  approaches its minimum, and towards this resonance point,  $\sigma(\tilde{\tau}_1 \tilde{\tau}_1^*)_{all}$  and  $R$  decrease significantly and show even a local minimum. This behavior is qualitatively different from the one shown in figure 3 (c) where the maximum of  $\sigma(\tilde{\tau}_1 \tilde{\tau}_1^*)_{all}$  is very close to the threshold for on-shell Higgs exchange,  $2m_{\tilde{\tau}_1} = m_{H^0}$ . The difference results from the kinematical cuts (4.1) applied in figure 13. As shown in figure 7, the  $b\bar{b}$  and  $gg$  channels lead to a significant excess of staus with low  $p^T$  and low  $\beta$  compared to the Drell–Yan channel in the vicinity of the resonance. Thus, by imposing the  $p^T$  and  $\beta$  cuts (4.1), one loses a significant amount of direct stau production events near the resonance condition  $2m_{\tilde{\tau}_1} = m_{H^0}$ .

For the CMSSM scans in figure 12, the above explains also that maximum values of  $R$  are shifted to some extent away from the  $2m_{\tilde{\tau}_1} \approx m_{H^0}$  region and deeper into the  $2m_{\tilde{\tau}_1} < m_{H^0}$  region when moving along contours of constant  $m_{\tilde{\tau}_1}$ . In fact, the dip at the resonance is present also in those scans but not visible due to a limited resolution.

Based on this finding and as already addressed in section 4.1, we would thus recommend a shifting of the  $p^T$  and  $\beta$  cuts to include events with smaller  $p^T$  and  $\beta$ . If this is feasible such that direct stau production events can still be identified confidently and if close to the resonance, one will find  $R$  values that increase substantially when lowering the cuts on  $p^T$  and  $\beta$ . Such a behavior can then provide a hint for resonant stau annihilation in the early Universe and thereby for the possibility of an exceptionally small  $Y_{\tilde{\tau}_1}$ . For further clarification, we propose in the following studies of differential direct stau production cross sections.

On the side, we remark that the mass scale of the heavy Higgs bosons is, by renormalization group running, fixed by  $m_{1/2}$  in NUHM1 models. Although we can always realize  $2m_{\tilde{\tau}_1} \approx m_{H^0}$  in NUHM1 models, these parameter points have a light  $\tilde{\tau}_1$  only for small  $m_{1/2}$ . Thus, one does not find scenarios with efficient direct stau production and subdominant indirect stau production from cascade decays. However, in the alternative less constrained NUHM2 models,  $m_{H_u}$  and  $m_{H_d}$  are chosen independently. These two parameters can be traded for the parameters  $m_A$  and  $\tan\beta$  at the low scale. In the context of direct stau production, this setup can effectively be described by the low scale parameters  $m_{\tilde{\tau}_1}$ ,  $m_A$ , and  $\tan\beta$  with implications shown in section 3. Now, the different stau production mechanism might ‘decouple’ and there is the possibility that direct production remains as the only relevant source for stau pairs at hadron colliders.

### With a little help from differential direct $\tilde{\tau}_1\tilde{\tau}_1^*$ production cross sections

So far our discussion in this section has focussed on the quantity  $R$  (and thereby on the integrated direct stau production cross section) and its possible dependence on the  $p^T$  and  $\beta$  cuts. Now, with long-lived staus, it will be a realistic possibility to measure also differential direct  $\tilde{\tau}_1\tilde{\tau}_1^*$  production cross sections such as the ones discussed in section 4.

For a situation with a sizeable value of  $R > 3$ , as encountered for points  $\alpha$  or  $\gamma$ , the situation is most promising since the differential distributions differ substantially from the Drell–Yan predictions and provide valuable additional information. Our results show that such a large  $R$  results from contributions of the  $b\bar{b}$  channel that become substantial near  $2m_{\tilde{\tau}_1} = m_{H^0}$ , *i.e.*, the threshold for on-shell  $H^0$  exchange. Manifestations of an on-shell  $H^0$  exchange that leads to the large  $R$  value will then show up in the invariant mass distribution of the directly produced stau pair in the form of a resonance peak at  $m_{\tilde{\tau}_1\tilde{\tau}_1^*} = m_{H^0}$ . Considering those  $m_{\tilde{\tau}_1\tilde{\tau}_1^*}$  distributions for the points  $\alpha$  and  $\gamma$  in figures 8 (a) and (c), respectively, this feature is clearly visible. As already explained in section 4.2, the associated  $m_{H^0}$  can then be extracted and compared to  $2m_{\tilde{\tau}_1}$  which marks also the minimum value of  $m_{\tilde{\tau}_1\tilde{\tau}_1^*}$  in such a distribution. In fact, the  $H^0$  resonance at point  $\gamma$  shows that  $m_{H^0}$  is still close to  $2m_{\tilde{\tau}_1}$  but too large to allow for highly efficient resonant primordial stau annihilation. This is different for point  $\alpha$  where the  $m_{H^0}$  resonance peak sits much closer to the minimum  $m_{\tilde{\tau}_1\tilde{\tau}_1^*}$  value. This tells us immediately that this is a scenario with

$2m_{\tilde{\tau}_1} \approx m_{H^0}$  and thus with the possibility of efficient resonant primordial stau annihilation. Moreover, the  $m_{\tilde{\tau}_1\tilde{\tau}_1^*}$  distribution provides us also with the width  $\Gamma_{H^0}$  which is an important input in calculations of  $Y_{\tilde{\tau}_1}$  in that region.

For more moderate values of  $R \simeq 2-3$ , it may still be possible to clarify the situation. If such an  $R$  value results from on-shell  $H^0$  exchange, again a  $H^0$  resonance peak will show up in the corresponding  $m_{\tilde{\tau}_1\tilde{\tau}_1^*}$  distribution so that the situation can be resolved as explained above. In the possible case that no resonance peak shows up in the  $m_{\tilde{\tau}_1\tilde{\tau}_1^*}$  distribution (even under excellent experimental conditions), the excess over the Drell–Yan prediction may be due to a  $2m_{\tilde{\tau}_1}$  value that is slightly above  $m_{H^0}$  so that on-shell  $H^0$  is just not possible. This is the situation encountered, *e.g.*, for  $m_0^H \simeq -820$  GeV in the NUHM1 model considered in figure 13. Here we still expect an excess of events over the Drell–Yan prediction towards the minimum  $m_{\tilde{\tau}_1\tilde{\tau}_1^*}$  value in the invariant mass distribution but—without a resonance peak—it will not be possible to determine  $m_{H^0}$  or  $\Gamma_{H^0}$  in experimental studies of direct stau production. Nevertheless, those quantities may still be accessible at the LHC, *e.g.*, via studies of associated  $b\bar{b}h^0/H^0$  production with  $h^0/H^0 \rightarrow \mu^+\mu^-$ , which will remain conceivable also for very heavy colored particles. In fact, these reactions are considered to be very promising for  $m_{H^0}$  measurements at the LHC, despite the relatively small  $\text{BR}(h^0/H^0 \rightarrow \mu^+\mu^-)$  [135]. If this is indeed feasible, the described shape of the  $m_{\tilde{\tau}_1\tilde{\tau}_1^*}$  distribution together with a finding of  $2m_{\tilde{\tau}_1} \approx m_{H^0}$  will then point to the possibility of an exceptionally small  $Y_{\tilde{\tau}_1}$ . In fact, also in case of a more sizeable  $R$ , a second independent determination of  $m_{H^0}$  in studies of other processes will provide an important consistency check and test whether the observed resonance is indeed associated with the  $H^0$  boson.

For a scenario with resonant primordial stau annihilation and the associated mass pattern  $2m_{\tilde{\tau}_1} \approx m_{H^0}$ , the differential distributions with respect to  $p^T$  and  $\beta$  will also provide valuable information, which is already evident from our discussion on the  $p^T$  and  $\beta$  cut dependence of  $R$  and from section 4.1. However, we would like to stress once more that these distributions are very different from the Drell–Yan prediction towards low  $p^T$  and low  $\beta$  values for both the  $2m_{\tilde{\tau}_1} < m_{H^0}$  case and the  $2m_{\tilde{\tau}_1} > m_{H^0}$  case. This can be seen explicitly in figure 7 for two different scenarios with  $|2m_{\tilde{\tau}_1} - m_{H^0}| = 10$  GeV.

The most challenging situation with respect to the testing of the viability of an exceptionally small  $Y_{\tilde{\tau}_1}$  is encountered for scenarios such as point  $\beta$ . Here the exceptional yield results only from enhanced stau-Higgs couplings. Again the  $m_{\tilde{\tau}_1\tilde{\tau}_1^*}$  distribution shows differences with respect to the Drell–Yan prediction as can be seen in figure 8(b). These are manifestations of the  $gg$  channel contribution: While the  $H^0$ -mediated processes lead to the  $H^0$  resonance peak at  $m_{\tilde{\tau}_1\tilde{\tau}_1^*} \simeq 760$  GeV, the excess that shows up over a wide  $m_{\tilde{\tau}_1\tilde{\tau}_1^*}$  range (and in particular towards lower  $m_{\tilde{\tau}_1\tilde{\tau}_1^*}$ ) results mainly from the  $h^0$ -mediated processes that benefit from the significantly enhanced  $\tilde{\tau}_1\tilde{\tau}_1^*h^0$  coupling. However, from this information alone, it will be very difficult to infer confidently that an exceptional  $Y_{\tilde{\tau}_1}$  is possible. Moreover, in our numerical studies, we find that the  $gg$  channel contribution usually does not lead to  $R > 2$  (*cf.* point  $\beta$  in table 3). Thus, one will have to rely on other investigations that are sensitive to large values of  $\tan\beta$ ,  $|\mu|$ , and/or  $|A_\tau|$ . As outlined in section 9 of ref. [74], some of those investigations provide additional motivation for a future linear collider at which processes such as  $e^+e^- \rightarrow \tilde{\tau}_1\tilde{\tau}_1^*h^0/H^0$  and  $\gamma\gamma \rightarrow \tilde{\tau}_1\tilde{\tau}_1^*h^0/H^0$  can

indeed allow for direct experimental determinations of the stau-Higgs couplings.

Experimental insights into  $\tan\beta$ ,  $|\mu|$ , and/or  $|A_\tau|$  will be relevant also for the scenarios with larger  $R$  discussed above since larger stau-Higgs couplings are associated with more efficient resonant primordial stau annihilation and thereby with smaller  $Y_{\tilde{\tau}_1}$ . Here analyses of the decays  $H^0 \rightarrow \tau\bar{\tau}/b\bar{b}$  and associated limits/findings in the  $m_A$ - $\tan\beta$  plane will be highly interesting [112, 113]. Equally exciting will be the outcome of the ongoing searches for the decay  $B_s \rightarrow \mu^+\mu^-$ , *e.g.*, at the LHCb experiment [136]. As can be seen in table 1, with a sensitivity to a  $\text{BR}(B_s \rightarrow \mu^+\mu^-)$  as small as  $10^{-8}$ , one will be able to test points such as  $\alpha$  and  $\beta$  which allow for an exceptionally small stau yield.

## 7. Conclusions

We have studied the direct hadronic production of a pair of staus  $\tilde{\tau}_1\tilde{\tau}_1^*$  within the MSSM. In addition to the well-known Drell–Yan process, we have considered  $\tilde{\tau}_1\tilde{\tau}_1^*$  production processes initiated by  $b\bar{b}$  annihilation and gluon fusion, with all third-generation mixing effects taken into account. This allows us to provide reliable predictions of hadronic slepton production at  $\mathcal{O}(\alpha_s^2\alpha^2)$ . These predictions are independent of the stau lifetime and applicable in  $\tilde{\chi}_1^0$  LSP scenarios with the  $\tilde{\tau}_1$  NLSP as well as in settings in which the  $\tilde{\tau}_1$  is long-lived.

In considerable parts of the MSSM parameter space, we find that the additional  $b\bar{b}$  and  $gg$  channels lead to a substantial enhancement of the direct stau production cross section over the NLO-QCD Drell–Yan prediction. This enhancement can be even larger than one order of magnitude. Particularly significant corrections are found when direct stau production can proceed via the exchange of an on-shell heavy CP-even Higgs boson  $H^0$  and when the left-right-stau mixing is sizeable. Moreover, the contributions of the  $b\bar{b}$  and  $gg$  channels are enhanced also in the case of large stau-Higgs couplings which are associated with large values of  $\tan\beta$ ,  $|\mu|$ , and/or  $|A_\tau|$  and thereby again with a sizeable left-right-stau mixing.

In cosmologically motivated scenarios with gravitino or axino dark matter, the stau can be the lightest SUSY particle within the MSSM. In an R-parity conserving setting, the stau will then typically be long-lived since it can only decay into the extremely weakly interacting gravitino or axino. Such long-lived staus can lead to the striking collider signature of a charged massive particle, *i.e.*, a slowly moving charged object with large transverse momentum. SM backgrounds to this signature originate only from slow moving muons and kinematical cuts on the velocity  $\beta$  and  $p^T$  are required to separate these backgrounds. For such scenarios, we have investigated differential distributions of the directly produced staus and the associated integrated cross sections after application of the kinematical cuts. Our findings show that staus from the  $b\bar{b}$  and  $gg$  channels are often softer and slower than those produced in the Drell–Yan channel. We thus recommend that experiments should try to soften their cuts to improve sensitivity to these additional channels. Here, a detailed study including detector effects should be performed to investigate the possible discovery reach and exclusion limits.

Once long-lived staus are observed at the LHC, one will be able to measure the stau mass  $m_{\tilde{\tau}_1}$  accurately, *e.g.*, in TOF measurements. A measurement of the direct stau pro-

duction cross section—if governed by Drell–Yan processes—will then probe the stau mixing angle  $\theta_{\tilde{\tau}}$ . However, we have shown that there is also the possibility of an early observation of a significant excess of the direct stau production cross section over the Drell–Yan prediction. Indeed, such a finding can be a first hint for Higgs physics at the LHC. Moreover, our results demonstrate that measurements of the distribution of direct stau production events as a function of the invariant stau-antistau mass  $m_{\tilde{\tau}_1\tilde{\tau}_1^*}$  can give  $m_{\tilde{\tau}_1}$ , independently, and, more importantly, the mass of the heavy CP-even Higgs boson  $m_{H^0}$ . Although challenging, with precise measurements of the invariant mass  $m_{\tilde{\tau}_1\tilde{\tau}_1^*}$ , we find that these distributions may provide us also with the Higgs width  $\Gamma_{H^0}$ . In fact, for large event samples, both the  $m_{H^0}$  and the  $\Gamma_{H^0}$  determination might even be possible in parameter regions in which direct stau production is governed by the Drell–Yan channels.

We have also presented results that are encouraging for the stopping of long-lived staus in the collider detectors [29, 40–42] or in additional surrounding material [30, 43–45]. With a large number of stopped staus, such experiments could allow for analyses of their late decays. Those analyses may give unique insights into the nature of the LSP into which the stau decays and into the vertex that governs this decay. In this way, it could be possible to use collider experiments to probe physics at scales as high as the Peccei–Quinn scale [28, 29] or the Planck scale [24]. A crucial criterium for the stopping of large numbers of staus is that a large fraction of them is produced with relatively slow initial velocities. This is exactly what we find if the staus are directly produced via the  $b\bar{b}$  and  $gg$  channels in the appealing scenarios in which the thermal relic stau abundance can be exceptionally small. Here the number of stopped directly produced staus may exceed expectations based on the Drell–Yan channels by more than one order of magnitude.

Within the CMSSM, we have provided cross section predictions for direct stau production at the LHC with  $\sqrt{S} = 7$  TeV and 14 TeV and at the Tevatron. Here our focus has been on a particular  $m_0$ - $m_{1/2}$  plane in which the long-lived staus can have an exceptionally small thermal relic stau abundance. For the considered scenarios with  $\tan\beta = 55$ , we predict substantial contributions from the  $b\bar{b}$  and  $gg$  channels in large areas of the  $m_0$ - $m_{1/2}$  plane. By comparing our results for the Tevatron with the associated existing upper limit of 10 fb, a small strip along the conservative lower stau mass limit from LEP of 82 GeV is found to be disfavored in that particular plane. On the other hand, our cross section predictions show that it will be difficult to discover directly produced staus with  $m_{\tilde{\tau}_1} \gtrsim 100$  GeV at the Tevatron. This is different for the LHC with  $\sqrt{S} = 7$  TeV where tests of direct stau production will be possible in the very near future. In particular, the CMSSM parameter region in which an exceptionally small stau yield is possible because of resonant primordial stau annihilation will be tested very soon.

To address the relative importance of direct stau production with respect to indirect stau production in cascade decays, we have considered four CMSSM benchmark points. Our calculations show that direct stau production can be one of the dominant contributions especially in the cosmologically motivated scenarios with an exceptionally small stau yield. Moreover, we find that the early LHC with  $\sqrt{S} = 7$  TeV may provide a better environment for the study of direct stau production than the LHC with  $\sqrt{S} = 14$  TeV at which indirect stau production is often expected to become dominant.

Finally, we have explored the testability of the conditions that allow for an exceptionally small stau yield at the LHC. Within the CMSSM and for a NUHM1 scenario, we have studied whether an excess of the direct stau production cross section over the Drell–Yan prediction can be used as an indicator for the possibility of an exceptional yield. Although no one-to-one link is found, a large excess over the Drell–Yan prediction can very well be a first hint of efficient stau annihilation in the early Universe. Additional investigations—especially in the Higgs sector—will still be crucial to clarify the situation. Important additional insights can be provided by studying the differential distributions of the directly produced  $\tilde{\tau}_1 \tilde{\tau}_1^*$  pairs. In particular, the differential distribution as a function of the invariant mass  $m_{\tilde{\tau}_1 \tilde{\tau}_1^*}$  may clarify the situation in a striking way: If the mentioned large excess is observed and if one is in the region that allows for efficient resonant primordial stau annihilation, in which  $2m_{\tilde{\tau}_1} \approx m_{H^0}$ , this  $m_{\tilde{\tau}_1 \tilde{\tau}_1^*}$  distribution will show a pronounced  $H^0$  resonance peak right at the beginning.

In summary, direct stau production including  $b\bar{b}$  and  $gg$  channels can be probed in the very near future or even with data already available. Once discovered, this process might shed light on SUSY parameters and important cosmological questions soon.

## Acknowledgments

We are grateful to T. Hahn, W. Hollik, J. Germer, P. Graf, and A. Landwehr for valuable discussions. This work was supported in part by the Cluster of Excellence “Origin and Structure of the Universe” and by the US DOE under contract No. DE-FG02-95ER40896.

## A. Stau sector in the MSSM

In this appendix we introduce the notation that we use to describe the stau sector in the MSSM, including the left-right mixing of the two stau mass eigenstates and stau-Higgs couplings.

### A.1 Stau mixing and mass eigenstates

After electroweak symmetry breaking the soft-breaking terms in the MSSM Lagrangian induce mixing between the left- and right-handed gauge eigenstates in the sfermion sector. Under the assumption of minimal flavor violation, the sfermion mass matrices and trilinear couplings are diagonal in family space and no mixing occurs amongst different flavors. Furthermore, we assume all parameters to be real. Including all F-term, D-term and soft-term contributions, the stau-mass-squared matrix then reads in the basis of gauge eigenstates  $(\tilde{\tau}_L, \tilde{\tau}_R)$ :

$$\mathcal{M}_{\tilde{\tau}}^2 = \begin{pmatrix} m_\tau^2 + m_{LL}^2 & m_\tau X_\tau \\ m_\tau X_\tau & m_\tau^2 + m_{RR}^2 \end{pmatrix} = (R_{\tilde{\tau}})^\dagger \begin{pmatrix} m_{\tilde{\tau}_1}^2 & 0 \\ 0 & m_{\tilde{\tau}_2}^2 \end{pmatrix} R_{\tilde{\tau}}, \quad (\text{A.1})$$



with

$$\begin{aligned}
m_{\tilde{L}\tilde{L}}^2 &= m_{\tilde{L}_3}^2 + \left(-\frac{1}{2} + \sin^2 \theta_W\right) M_Z^2 \cos 2\beta, \\
m_{\tilde{R}\tilde{R}}^2 &= m_{\tilde{E}_3}^2 - \sin^2 \theta_W M_Z^2 \cos 2\beta, \\
X_\tau &= A_\tau - \mu \tan \beta.
\end{aligned} \tag{A.2}$$

Here,  $m_{\tilde{L}_3}$  and  $m_{\tilde{E}_3}$  are the left-handed and right-handed stau soft-breaking masses and  $A_\tau$  is the trilinear coupling in the stau sector,  $\mu$  the Higgs-higgsino mass parameter, and  $\tan \beta = v_2/v_1$  the ratio of the two Higgs vacuum expectation values. As indicated in (A.1), the stau mixing matrix can be diagonalized by an orthogonal  $2 \times 2$  matrix  $R_{\tilde{\tau}}$ , parametrized by the stau mixing angle  $\theta_{\tilde{\tau}}$ ,

$$R_{\tilde{\tau}} = \begin{pmatrix} \cos \theta_{\tilde{\tau}} & \sin \theta_{\tilde{\tau}} \\ -\sin \theta_{\tilde{\tau}} & \cos \theta_{\tilde{\tau}} \end{pmatrix}, \tag{A.3}$$

and the stau mass eigenvalues squared are given by

$$m_{\tilde{\tau}_1, \tilde{\tau}_2}^2 = m_\tau^2 + \frac{1}{2} \left[ m_{\tilde{R}\tilde{R}}^2 + m_{\tilde{L}\tilde{L}}^2 \mp \sqrt{(m_{\tilde{L}\tilde{L}}^2 - m_{\tilde{R}\tilde{R}}^2)^2 + 4m_\tau^2 X_\tau^2} \right]. \tag{A.4}$$

By convention  $R_{\tilde{\tau}}$  is chosen such that  $\tilde{\tau}_1$  is the lighter of the two eigenstates. Imposing this requirement and choosing  $0 \leq \theta_{\tilde{\tau}} < \pi$ , the mixing angle is determined by

$$\tan 2\theta_{\tilde{\tau}} = \frac{2m_\tau X_\tau}{m_{\tilde{L}\tilde{L}}^2 - m_{\tilde{R}\tilde{R}}^2}, \quad \text{and} \quad \sin 2\theta_{\tilde{\tau}} = \frac{2m_\tau X_\tau}{m_{\tilde{\tau}_1}^2 - m_{\tilde{\tau}_2}^2}. \tag{A.5}$$

For a mixing angle of  $\theta_{\tilde{\tau}} = \pi/2$  (0),  $\tilde{\tau}_1$  is purely right(left)-handed, while maximal mixing occurs for  $\theta_{\tilde{\tau}} = \pi/4$  and  $3\pi/4$ .

Equation (A.5) gives a direct relation between the mixing angle, the off-diagonal parameter  $X_\tau$  and the gauge eigenstates ( $\tilde{\tau}_L, \tilde{\tau}_R$ ) or mass eigenstates ( $\tilde{\tau}_1, \tilde{\tau}_2$ ). Thus, in section 3 and partly in section 4, we use  $m_{\tilde{\tau}_1}$  and  $\theta_{\tilde{\tau}}$  as input parameters, together with  $A_\tau$ ,  $\mu$ , and  $\tan \beta$ , to determine the heavier stau mass  $m_{\tilde{\tau}_2}$  and then compute  $m_{\tilde{L}_3}$  and  $m_{\tilde{E}_3}$  from (A.1). Furthermore, by  $SU(2)_L$  invariance,  $m_{\tilde{L}_3}$  then sets the mass of the tau-sneutrino,  $m_{\tilde{\nu}_\tau}$ .

## A.2 Stau-Higgs couplings

In the minimal flavor violating MSSM, the sfermions couple directly to the Higgs fields via dimensionful parameters. The stau-Higgs couplings are given by [137]

$$\mathcal{L}_{\tilde{\tau}\tilde{\tau}\mathcal{H}} = \frac{g}{M_W} \sum_{I,J=L,R} \tilde{\tau}_I^* \tilde{C}[\tilde{\tau}_I^*, \tilde{\tau}_J, \mathcal{H}] \tilde{\tau}_J \mathcal{H}, \tag{A.6}$$

where  $\mathcal{H}$  stands for any of the neutral Higgs and Goldstone bosons,  $\mathcal{H} = h^0, H^0, A^0, G^0$ . In the basis of the gauge eigenstates ( $\tilde{\tau}_L, \tilde{\tau}_R$ ), the reduced coupling  $\tilde{C}[\tilde{\tau}_I^*, \tilde{\tau}_J, h^0]$  reads

$$\tilde{C}[\tilde{\tau}_I^*, \tilde{\tau}_J, h^0] = \begin{pmatrix} -\frac{\cos 2\theta_W}{2} M_Z^2 s_{\alpha+\beta} + m_\tau^2 \frac{s_\alpha}{c_\beta} & \frac{m_\tau}{2} \left( A_\tau \frac{s_\alpha}{c_\beta} + \mu \frac{c_\alpha}{c_\beta} \right) \\ \frac{m_\tau}{2} \left( A_\tau \frac{s_\alpha}{c_\beta} + \mu \frac{c_\alpha}{c_\beta} \right) & -\sin^2 \theta_W M_Z^2 s_{\alpha+\beta} + m_\tau^2 \frac{s_\alpha}{c_\beta} \end{pmatrix}, \tag{A.7}$$

and  $\tilde{C}[\tilde{\tau}_I^*, \tilde{\tau}_J, H^0]$  can be obtained upon the replacement  $\alpha \rightarrow \alpha - \pi/2$ , where  $\alpha$  is the Higgs scalar mixing angle. Here and below, the shorthand notation  $c_\gamma \equiv \cos \gamma$  and  $s_\gamma \equiv \sin \gamma$  (with  $\gamma = \alpha, \beta, \theta_{\tilde{\tau}}$ ) is used. The reduced coupling for the CP-odd Higgs boson  $A^0$  reads

$$\tilde{C}[\tilde{\tau}_I^*, \tilde{\tau}_J, A^0] = \begin{pmatrix} 0 & +i \frac{m_\tau}{2} (A_\tau \tan \beta + \mu) \\ -i \frac{m_\tau}{2} (A_\tau \tan \beta + \mu) & 0 \end{pmatrix}, \quad (\text{A.8})$$

and  $\tilde{C}[\tilde{\tau}_I^*, \tilde{\tau}_J, G^0]$  can be obtained upon the replacement:  $A_\tau \tan \beta + \mu \rightarrow \mu \tan \beta - A_\tau$ .

We are particularly interested in the couplings between the lighter mass eigenstate  $\tilde{\tau}_1$  and the CP-even Higgs bosons  $h^0$  and  $H^0$ . These can be found by diagonalizing the coupling matrix in (A.7) with the orthogonal matrix  $R_{\tilde{\tau}}$  defined in (A.3):

$$C[\tilde{\tau}_1^*, \tilde{\tau}_1, h^0] = \left( -\frac{1}{2} c_{\theta_{\tilde{\tau}}}^2 + \sin^2 \theta_W c_{2\theta_{\tilde{\tau}}} \right) M_Z^2 s_{\alpha+\beta} + m_\tau^2 \frac{s_\alpha}{c_\beta} + \frac{m_\tau}{2} \left( A_\tau \frac{s_\alpha}{c_\beta} + \mu \frac{c_\alpha}{c_\beta} \right) s_{2\theta_{\tilde{\tau}}}. \quad (\text{A.9})$$

The coupling  $C[\tilde{\tau}_1^*, \tilde{\tau}_1, H^0]$  can be read from (A.9) after the replacement  $\alpha \rightarrow \alpha - \pi/2$ . Thus, the SUSY parameters  $\mu$  and  $A_\tau$  enter proportional to  $\sin 2\theta_{\tilde{\tau}}$  and the coupling peaks at  $\theta_{\tilde{\tau}} = \pi/4$ . This holds analogously for the  $\tilde{\tau}_1^* \tilde{\tau}_1 H^0$  coupling, whereas the diagonal coupling to the CP-odd Higgs boson  $A^0$  vanishes:  $C[\tilde{\tau}_1^*, \tilde{\tau}_1, A^0] = 0$ .

## B. Resummation in the bottom sector

The Higgs sector in the MSSM corresponds to a type-II two-Higgs doublet model, where the down-type quarks couple to  $H_1$  and the up-type quarks to  $H_2$ . After spontaneous symmetry breaking, the up- (down-)type quarks gain masses by coupling to the non-zero  $H_2$  ( $H_1$ ) vacuum expectation values  $v_2$  ( $v_1$ ). At tree-level, the bottom-quark mass  $m_b$  is given by

$$m_b = \lambda_b v_1, \quad (\text{B.1})$$

where  $\lambda_b$  is the  $b\bar{b}H_1$  Yukawa coupling. However radiative corrections induce an effective  $b\bar{b}H_2$  coupling that can significantly alter the tree-level relation [118–122]. These higher-order contributions do not decouple at low energies and are enhanced by a factor  $\tan \beta = v_2/v_1$ ,

$$\begin{aligned} m_b &= \lambda_b v_1 + \Delta \lambda_b v_2 = \lambda_b v_1 \left( 1 + \frac{\Delta \lambda_b}{\lambda_b} \tan \beta \right) \\ &\equiv \lambda_b v_1 (1 + \Delta m_b). \end{aligned} \quad (\text{B.2})$$

As shown in ref. [122], the leading  $\tan \beta$  enhanced terms can be resummed to all orders and easiest be implemented by using an effective bottom-quark Yukawa coupling  $\lambda_b^{\text{eff}} \equiv m_b^{\text{eff}}/v_1$ . The dominant contributions to  $\Delta m_b$  arise from gluino-sbottom and chargino-stop loops,

$$\Delta m_b = \frac{2\alpha_s}{3\pi} M_3 \mu \tan \beta I(m_{\tilde{b}_1}, m_{\tilde{b}_2}, m_{\tilde{g}}) + \frac{\lambda_t^2}{16\pi^2} \mu A_t \tan \beta I(m_{\tilde{t}_1}, m_{\tilde{t}_2}, \mu), \quad (\text{B.3})$$

with the gluino mass  $M_3$ , the lighter (heavier) sbottom mass  $m_{\tilde{b}_1}$  ( $m_{\tilde{b}_2}$ ) the trilinear coupling  $A_t$  in the stop sector, the lighter (heavier) stop mass  $m_{\tilde{t}_1}$  ( $m_{\tilde{t}_2}$ ), and the loop function

$$I(a, b, c) = \frac{1}{(a^2 - b^2)(b^2 - c^2)(a^2 - c^2)} \left[ a^2 b^2 \log \frac{a^2}{b^2} + b^2 c^2 \log \frac{b^2}{c^2} + c^2 a^2 \log \frac{c^2}{a^2} \right]. \quad (\text{B.4})$$

Further neutralino-sbottom contributions are proportional to the weak coupling  $g^2$  and subdominant only.

Here we follow refs. [123, 138] and use a  $\overline{\text{DR}}$  definition of the effective mass to take large logarithms from the running Yukawa coupling into account. The effective Yukawa coupling  $\lambda_b^{\text{eff}}$  is then defined as follows,

$$\lambda_b^{\text{eff}} = \frac{1}{v_1} \frac{m_b^{\overline{\text{DR}}}(\mu_R) + m_b \Delta m_b}{1 + \Delta m_b} \equiv \frac{m_b^{\overline{\text{DR}}, \text{eff}}}{v_1}, \quad (\text{B.5})$$

where the second term in the numerator is necessary to avoid double counting of the resummed terms. The  $\overline{\text{DR}}$  bottom mass at the renormalization scale  $\mu_R$  can be obtained from the on-shell bottom-quark mass,  $m_b^{\text{OS}}$ , and the UV-finite parts of the bottom-quark self-energy (here in Lorentz decomposition),

$$m_b^{\overline{\text{DR}}}(\mu_R) = m_b^{\text{OS}} + \frac{m_b}{2} \left( \Sigma_L^{\text{fin.}}(m_b) + \Sigma_R^{\text{fin.}}(m_b) + 2 \Sigma_S^{\text{fin.}}(m_b) \right), \quad (\text{B.6})$$

with

$$m_b^{\text{OS}} = m_b^{\overline{\text{MS}}}(M_Z) b^{\text{shift}}, \quad b^{\text{shift}} = 1 + \frac{\alpha_s}{\pi} \left( \frac{4}{3} - \log \frac{[m_b^{\overline{\text{MS}}}(M_Z)]^2}{M_Z^2} \right). \quad (\text{B.7})$$

Further  $\tan \beta$  enhancement effects arise in the trilinear couplings involving Higgs–bottom interactions. They can be resummed and taken into account by modifying the  $b\bar{b}\mathcal{H}$  coupling  $g_{b\bar{b}\mathcal{H}}$ . The combined effect of the resummation in the relation between  $\lambda_b$  and  $m_b$  and of the resummation in the Higgs–bottom vertices is accounted for by performing the following substitutions in the couplings,

$$\begin{aligned} g_{bbh^0} &\rightarrow g_{bbh^0} \Big|_{\lambda_b \rightarrow \lambda_b^{\text{eff}}} \left( 1 - \frac{\Delta m_b}{\tan \beta \tan \alpha} \right), & g_{bbA^0} &\rightarrow g_{bbA^0} \Big|_{\lambda_b \rightarrow \lambda_b^{\text{eff}}} \left( 1 - \frac{\Delta m_b}{\tan^2 \beta} \right), \\ g_{bbH^0} &\rightarrow g_{bbH^0} \Big|_{\lambda_b \rightarrow \lambda_b^{\text{eff}}} \left( 1 + \Delta m_b \frac{\tan \alpha}{\tan \beta} \right), & g_{bbG^0} &\rightarrow g_{bbG^0}. \end{aligned} \quad (\text{B.8})$$

The coupling involving the Goldstone boson  $G^0$  is not modified since the contribution from the vertex corrections exactly compensates the contribution of the bottom–Yukawa coupling resummation.

## References

- [1] J. Wess and J. Bagger, *Supersymmetry and supergravity*. 1992. Princeton, USA: Univ. Pr. 259 p.
- [2] H. P. Nilles, *Supersymmetry, Supergravity and Particle Physics*, *Phys. Rept.* **110** (1984) 1–162.

- [3] H. E. Haber and G. L. Kane, *The Search for Supersymmetry: Probing Physics Beyond the Standard Model*, *Phys. Rept.* **117** (1985) 75–263.
- [4] S. P. Martin, *A supersymmetry primer*, [hep-ph/9709356](#).
- [5] M. Drees, R. Godbole, and P. Roy, *Theory and Phenomenology of Sparticles: An account of four-dimensional  $N=1$  supersymmetry in high energy physics*. 2004. Hackensack, USA: World Scientific 555 p.
- [6] H. Baer and X. Tata, *Weak scale supersymmetry: From superfields to scattering events*. 2006. Cambridge, UK: Univ. Pr. 537 p.
- [7] G. Jungman, M. Kamionkowski, and K. Griest, *Supersymmetric dark matter*, *Phys. Rept.* **267** (1996) 195–373, [[hep-ph/9506380](#)].
- [8] E. A. Baltz, M. Battaglia, M. E. Peskin, and T. Wizansky, *Determination of dark matter properties at high-energy colliders*, *Phys. Rev.* **D74** (2006) 103521, [[hep-ph/0602187](#)].
- [9] F. D. Steffen, *Dark Matter Candidates - Axions, Neutralinos, Gravitinos, and Axinos*, *Eur. Phys. J.* **C59** (2009) 557–588, [[arXiv:0811.3347](#)].
- [10] **CMS** Collaboration, V. Khachatryan *et. al.*, *Search for Supersymmetry in  $pp$  Collisions at 7 TeV in Events with Jets and Missing Transverse Energy*, *Phys. Lett.* **B698** (2011) 196–218, [[arXiv:1101.1628](#)].
- [11] **ATLAS** Collaboration, J. B. G. da Costa *et. al.*, *Search for squarks and gluinos using final states with jets and missing transverse momentum with the ATLAS detector in  $\sqrt{s} = 7$  TeV proton-proton collisions*, [arXiv:1102.5290](#).
- [12] P. Bechtle *et. al.*, *What if the LHC does not find supersymmetry in the  $\sqrt{s} = 7$  TeV run?*, [arXiv:1102.4693](#).
- [13] J. R. Ellis, T. Falk, K. A. Olive, and M. Srednicki, *Calculations of neutralino-stau coannihilation channels and the cosmologically relevant region of MSSM parameter space*, *Astropart.Phys.* **13** (2000) 181–213, [[hep-ph/9905481](#)].
- [14] **Particle Data Group** Collaboration, K. Nakamura *et. al.*, *Review of particle physics*, *J.Phys.* **G37** (2010) 075021.
- [15] A. Akeroyd, M. A. Diaz, J. Ferrandis, M. Garcia-Jareno, and J. Valle, *Charged Higgs boson and Stau phenomenology in the simplest  $R$  parity breaking model*, *Nucl.Phys.* **B529** (1998) 3–22, [[hep-ph/9707395](#)].
- [16] B. Allanach, A. Dedes, and H. Dreiner,  *$R$  parity violating minimal supergravity model*, *Phys.Rev.* **D69** (2004) 115002, [[hep-ph/0309196](#)].
- [17] W. Buchmüller, L. Covi, K. Hamaguchi, A. Ibarra, and T. Yanagida, *Gravitino dark matter in  $r$ -parity breaking vacua*, *JHEP* **03** (2007) 037, [[hep-ph/0702184](#)].
- [18] H. K. Dreiner, S. Grab, and M. K. Trenkel, *Stau LSP Phenomenology: Two versus Four-Body Decay Modes. Example: Resonant Single Slepton Production at the LHC*, *Phys. Rev.* **D79** (2009) 016002, [[arXiv:0808.3079](#)].
- [19] K. Desch, S. Fleischmann, P. Wienemann, H. K. Dreiner, and S. Grab, *Stau as the Lightest Supersymmetric Particle in  $R$ -Parity Violating SUSY Models: Discovery Potential with Early LHC Data*, *Phys. Rev.* **D83** (2011) 015013, [[arXiv:1008.1580](#)].

- [20] S. Ambrosanio, G. D. Kribs, and S. P. Martin, *Signals for gauge-mediated supersymmetry breaking models at the CERN LEP2 collider*, *Phys. Rev.* **D56** (1997) 1761–1777, [[hep-ph/9703211](#)].
- [21] J. L. Feng and T. Moroi, *Tevatron Signatures of Long-lived Charged Sleptons in Gauge-Mediated Supersymmetry Breaking Models*, *Phys. Rev.* **D58** (1998) 035001, [[hep-ph/9712499](#)].
- [22] S. P. Martin and J. D. Wells, *Cornering gauge-mediated supersymmetry breaking with quasi-stable sleptons at the Tevatron*, *Phys. Rev.* **D59** (1999) 035008, [[hep-ph/9805289](#)].
- [23] S. Ambrosanio, B. Mele, S. Petrarca, G. Polesello, and A. Rimoldi, *Measuring the SUSY breaking scale at the LHC in the slepton NLSP scenario of GMSB models*, *JHEP* **01** (2001) 014, [[hep-ph/0010081](#)].
- [24] W. Buchmüller, K. Hamaguchi, M. Ratz, and T. Yanagida, *Supergravity at colliders*, *Phys. Lett.* **B588** (2004) 90–98, [[hep-ph/0402179](#)].
- [25] F. D. Steffen, *Gravitino dark matter and cosmological constraints*, *JCAP* **0609** (2006) 001, [[hep-ph/0605306](#)].
- [26] J. R. Ellis, A. R. Raklev, and O. K. Oye, *Gravitino dark matter scenarios with massive metastable charged sparticles at the LHC*, *JHEP* **0610** (2006) 061, [[hep-ph/0607261](#)].
- [27] L. Covi, L. Roszkowski, R. Ruiz de Austri, and M. Small, *Axino dark matter and the CMSSM*, *JHEP* **06** (2004) 003, [[hep-ph/0402240](#)].
- [28] A. Brandenburg, L. Covi, K. Hamaguchi, L. Roszkowski, and F. D. Steffen, *Signatures of axinos and gravitinos at colliders*, *Phys. Lett.* **B617** (2005) 99–111, [[hep-ph/0501287](#)].
- [29] A. Freitas, F. D. Steffen, N. Tajuddin, and D. Wyler, *Axinos in Cosmology and at Colliders*, *JHEP* **1106** (2011) 036, [[arXiv:1105.1113](#)].
- [30] K. Hamaguchi, Y. Kuno, T. Nakaya, and M. M. Nojiri, *A Study of late decaying charged particles at future colliders*, *Phys.Rev.* **D70** (2004) 115007, [[hep-ph/0409248](#)].
- [31] K. Ishiwata, T. Ito, and T. Moroi, *Long-Lived Unstable Superparticles at the LHC*, *Phys.Lett.* **B669** (2008) 28–33, [[arXiv:0807.0975](#)].
- [32] S. Biswas and B. Mukhopadhyaya, *Chargino reconstruction in supersymmetry with long-lived staus*, *Phys.Rev.* **D81** (2010) 015003, [[arXiv:0910.3446](#)].
- [33] J. L. Feng, S. T. French, I. Galon, C. G. Lester, Y. Nir, *et. al.*, *Measuring Slepton Masses and Mixings at the LHC*, *JHEP* **1001** (2010) 047, [[arXiv:0910.1618](#)].
- [34] T. Ito, R. Kitano, and T. Moroi, *Measurement of the Superparticle Mass Spectrum in the Long-Lived Stau Scenario at the LHC*, *JHEP* **1004** (2010) 017, [[arXiv:0910.5853](#)].
- [35] J. J. Heckman, J. Shao, and C. Vafa, *F-theory and the LHC: Stau Search*, *JHEP* **1009** (2010) 020, [[arXiv:1001.4084](#)].
- [36] R. Kitano and M. Nakamura, *Tau polarization measurements at the LHC in supersymmetric models with a long-lived stau*, *Phys.Rev.* **D82** (2010) 035007, [[arXiv:1006.2904](#)].
- [37] T. Ito and T. Moroi, *Spin and Chirality Determination of Superparticles with Long-Lived Stau at the LHC*, *Phys.Lett.* **B694** (2011) 349–354, [[arXiv:1007.3060](#)].
- [38] T. Ito, *Squark Mass Measurement in the Long-lived Stau Scenario at the LHC*, *Phys.Lett.* **B699** (2011) 151–157, [[arXiv:1012.1318](#)].

- [39] S. Asai, Y. Azuma, M. Endo, K. Hamaguchi, and S. Iwamoto, *Stau Kinks at the LHC*, [arXiv:1103.1881](#).
- [40] H.-U. Martyn, *Detecting metastable staus and gravitinos at the ILC*, *Eur.Phys.J.* **C48** (2006) 15–24, [[hep-ph/0605257](#)].
- [41] S. Asai, K. Hamaguchi, and S. Shirai, *Measuring lifetimes of long-lived charged massive particles stopped in LHC detectors*, *Phys.Rev.Lett.* **103** (2009) 141803, [[arXiv:0902.3754](#)].
- [42] J. Pinfold and L. Sibley, *Measuring the Lifetime of Trapped Sleptons Using the General Purpose LHC Detectors*, *Phys.Rev.* **D83** (2011) 035021, [[arXiv:1006.3293](#)].
- [43] J. Goity, W. Kossler, and M. Sher, *Production, collection and utilization of very longlived heavy charged leptons*, *Phys.Rev.* **D48** (1993) 5437–5439, [[hep-ph/9305244](#)].
- [44] J. L. Feng and B. T. Smith, *Slepton trapping at the Large Hadron and International Linear Colliders*, *Phys. Rev.* **D71** (2005) 015004, [[hep-ph/0409278](#)].
- [45] K. Hamaguchi, M. M. Nojiri, and A. de Roeck, *Prospects to study a long-lived charged next lightest supersymmetric particle at the LHC*, *JHEP* **0703** (2007) 046, [[hep-ph/0612060](#)].
- [46] R. H. Cyburt, J. R. Ellis, B. D. Fields, and K. A. Olive, *Updated nucleosynthesis constraints on unstable relic particles*, *Phys.Rev.* **D67** (2003) 103521, [[astro-ph/0211258](#)].
- [47] M. Kawasaki, K. Kohri, and T. Moroi, *Big-Bang nucleosynthesis and hadronic decay of long-lived massive particles*, *Phys.Rev.* **D71** (2005) 083502, [[astro-ph/0408426](#)].
- [48] K. Jedamzik, *Big bang nucleosynthesis constraints on hadronically and electromagnetically decaying relic neutral particles*, *Phys.Rev.* **D74** (2006) 103509, [[hep-ph/0604251](#)].
- [49] M. Kawasaki, K. Kohri, T. Moroi, and A. Yotsuyanagi, *Big-Bang Nucleosynthesis and Gravitino*, *Phys.Rev.* **D78** (2008) 065011, [[arXiv:0804.3745](#)].
- [50] M. Pospelov, *Particle physics catalysis of thermal big bang nucleosynthesis*, *Phys. Rev. Lett.* **98** (2007) 231301, [[hep-ph/0605215](#)].
- [51] R. H. Cyburt, J. R. Ellis, B. D. Fields, K. A. Olive, and V. C. Spanos, *Bound-State Effects on Light-Element Abundances in Gravitino Dark Matter Scenarios*, *JCAP* **0611** (2006) 014, [[astro-ph/0608562](#)].
- [52] K. Hamaguchi, T. Hatsuda, M. Kamimura, Y. Kino, and T. Yanagida, *Stau-catalyzed Li-6 Production in Big-Bang Nucleosynthesis*, *Phys.Lett.* **B650** (2007) 268–274, [[hep-ph/0702274](#)].
- [53] J. Pradler and F. D. Steffen, *Implications of Catalyzed BBN in the CMSSM with Gravitino Dark Matter*, *Phys. Lett.* **B666** (2008) 181–184, [[arXiv:0710.2213](#)].
- [54] M. Pospelov, *Bridging the primordial A=8 divide with Catalyzed Big Bang Nucleosynthesis*, [arXiv:0712.0647](#).
- [55] M. Pospelov, J. Pradler, and F. D. Steffen, *Constraints on Supersymmetric Models from Catalytic Primordial Nucleosynthesis of Beryllium*, *JCAP* **0811** (2008) 020, [[arXiv:0807.4287](#)].
- [56] F. D. Steffen, *Constraints on Gravitino Dark Matter Scenarios with Long-Lived Charged Sleptons*, *AIP Conf. Proc.* **903** (2007) 595–598, [[hep-ph/0611027](#)].
- [57] J. Pradler and F. D. Steffen, *Constraints on the reheating temperature in gravitino dark matter scenarios*, *Phys. Lett.* **B648** (2007) 224–235, [[hep-ph/0612291](#)].

- [58] J. Kersten and K. Schmidt-Hoberg, *The Gravitino-Stau Scenario after Catalyzed BBN*, *JCAP* **0801** (2008) 011, [[arXiv:0710.4528](#)].
- [59] J. Pradler and F. D. Steffen, *CBBN in the CMSSM*, *Eur. Phys. J.* **C56** (2008) 287–291, [[arXiv:0710.4548](#)].
- [60] S. Bailly, K. Jedamzik, and G. Moulhaka, *Gravitino Dark Matter and the Cosmic Lithium Abundances*, *Phys. Rev.* **D80** (2009) 063509, [[arXiv:0812.0788](#)].
- [61] A. Freitas, F. D. Steffen, N. Tajuddin, and D. Wyler, *Upper Limits on the Peccei-Quinn Scale and on the Reheating Temperature in Axino Dark Matter Scenarios*, *Phys. Lett.* **B679** (2009) 270–277, [[arXiv:0904.3218](#)].
- [62] M. Bolz, A. Brandenburg, and W. Buchmuller, *Thermal production of gravitinos*, *Nucl.Phys.* **B606** (2001) 518–544, [[hep-ph/0012052](#)].
- [63] A. Brandenburg and F. D. Steffen, *Axino dark matter from thermal production*, *JCAP* **0408** (2004) 008, [[hep-ph/0405158](#)].
- [64] J. Pradler and F. D. Steffen, *Thermal gravitino production and collider tests of leptogenesis*, *Phys.Rev.* **D75** (2007) 023509, [[hep-ph/0608344](#)].
- [65] V. S. Rychkov and A. Strumia, *Thermal production of gravitinos*, *Phys.Rev.* **D75** (2007) 075011, [[hep-ph/0701104](#)].
- [66] A. Strumia, *Thermal production of Axino Dark Matter*, *JHEP* **06** (2010) 036, [[arXiv:1003.5847](#)].
- [67] K. J. Bae, K. Choi, and S. H. Im, *Effective interactions of axion supermultiplet and thermal production of axino dark matter*, [arXiv:1106.2452](#).
- [68] M. Fukugita and T. Yanagida, *Baryogenesis without Grand Unification*, *Phys.Lett.* **B174** (1986) 45.
- [69] S. Davidson and A. Ibarra, *A Lower bound on the right-handed neutrino mass from leptogenesis*, *Phys.Lett.* **B535** (2002) 25–32, [[hep-ph/0202239](#)].
- [70] W. Buchmuller, P. Di Bari, and M. Plumacher, *Leptogenesis for pedestrians*, *Annals Phys.* **315** (2005) 305–351, [[hep-ph/0401240](#)].
- [71] S. Blanchet and P. Di Bari, *Flavor effects on leptogenesis predictions*, *JCAP* **0703** (2007) 018, [[hep-ph/0607330](#)].
- [72] S. Antusch and A. Teixeira, *Towards constraints on the SUSY seesaw from flavour-dependent leptogenesis*, *JCAP* **0702** (2007) 024, [[hep-ph/0611232](#)].
- [73] M. Ratz, K. Schmidt-Hoberg, and M. W. Winkler, *A Note on the primordial abundance of stau NLSPs*, *JCAP* **0810** (2008) 026, [[arXiv:0808.0829](#)].
- [74] J. Pradler and F. D. Steffen, *Thermal relic abundances of long-lived staus*, *Nucl.Phys.* **B809** (2009) 318–346, [[arXiv:0808.2462](#)].
- [75] E. Eichten, I. Hinchliffe, K. D. Lane, and C. Quigg, *Super Collider Physics*, *Rev.Mod.Phys.* **56** (1984) 579–707.
- [76] H. Baer, B. Harris, and M. H. Reno, *Next-to-leading order slepton pair production at hadron colliders*, *Phys.Rev.* **D57** (1998) 5871–5874, [[hep-ph/9712315](#)].

- [77] W. Beenakker, M. Klasen, M. Kramer, T. Plehn, M. Spira, *et. al.*, *The Production of charginos / neutralinos and sleptons at hadron colliders*, *Phys.Rev.Lett.* **83** (1999) 3780–3783, [[hep-ph/9906298](#)].
- [78] G. Bozzi, B. Fuks, and M. Klasen, *Transverse-momentum resummation for slepton-pair production at the LHC*, *Phys. Rev.* **D74** (2006) 015001, [[hep-ph/0603074](#)].
- [79] G. Bozzi, B. Fuks, and M. Klasen, *Threshold Resummation for Slepton-Pair Production at Hadron Colliders*, *Nucl. Phys.* **B777** (2007) 157–181, [[hep-ph/0701202](#)].
- [80] G. Bozzi, B. Fuks, and M. Klasen, *Joint resummation for slepton pair production at hadron colliders*, *Nucl. Phys.* **B794** (2008) 46–60, [[arXiv:0709.3057](#)].
- [81] <http://www.thphys.uni-heidelberg.de/~plehn/prospino/> or <http://people.web.psi.ch/spira/prospino/>.
- [82] F. del Aguila and L. Ametller, *On the detectability of sleptons at large hadron colliders*, *Phys.Lett.* **B261** (1991) 326–333.
- [83] M. Bisset, S. Raychaudhuri, and P. Roy, *Higgs mediated slepton pair production at the large hadron collider*, [hep-ph/9602430](#).
- [84] F. Borzumati and K. Hagiwara, *Testing supersymmetry at the LHC through gluon-fusion production of a slepton pair*, *JHEP* **1103** (2011) 103, [[arXiv:0912.0454](#)].
- [85] T. Sjostrand *et. al.*, *High-energy physics event generation with PYTHIA 6.1*, *Comput. Phys. Commun.* **135** (2001) 238–259, [[hep-ph/0010017](#)].
- [86] G. Corcella *et. al.*, *HERWIG 6.5: an event generator for Hadron Emission Reactions With Interfering Gluons (including supersymmetric processes)*, *JHEP* **01** (2001) 010, [[hep-ph/0011363](#)].
- [87] N. Tajuddin, *Axinos in the Sky and on Earth*, *PhD Thesis, University of Zürich* (2010).
- [88] H. Baer, S. Kraml, A. Lessa, and S. Sekmen, *Thermal leptogenesis and the gravitino problem in the Asaka-Yanagida axion/axino dark matter scenario*, *JCAP* **1104** (2011) 039, [[arXiv:1012.3769](#)].
- [89] C. Cheung, G. Elor, and L. J. Hall, *The Cosmological Axino Problem*, [arXiv:1104.0692](#).
- [90] G. G. Raffelt, *Astrophysical axion bounds*, *Lect. Notes Phys.* **741** (2008) 51–71, [[hep-ph/0611350](#)].
- [91] M. Drees and X. Tata, *Signals for heavy exotics at hadron colliders and supercolliders*, *Phys.Lett.* **B252** (1990) 695–702.
- [92] A. Nisati, S. Petrarca, and G. Salvini, *On the possible detection of massive stable exotic particles at the LHC*, *Mod.Phys.Lett.* **A12** (1997) 2213–2222, [[hep-ph/9707376](#)].
- [93] M. Fairbairn, A. Kraan, D. Milstead, T. Sjostrand, P. Z. Skands, *et. al.*, *Stable massive particles at colliders*, *Phys.Rept.* **438** (2007) 1–63, [[hep-ph/0611040](#)].
- [94] J. L. Feng, M. Kamionkowski, and S. K. Lee, *Light Gravitinos at Colliders and Implications for Cosmology*, *Phys.Rev.* **D82** (2010) 015012, [[arXiv:1004.4213](#)].
- [95] **LEP2 SUSY Working Group** Collaboration, *Combined LEP GMSB Stau/Smuon/Selectron Results, 189-208 GeV, .*  
[http://lepsusy.web.cern.ch/lepsusy/www/gmsb\\_summer02/lepgmsb.html](http://lepsusy.web.cern.ch/lepsusy/www/gmsb_summer02/lepgmsb.html).



- [96] **D0** Collaboration, V. Abazov *et. al.*, *Search for Long-Lived Charged Massive Particles with the D0 Detector*, *Phys.Rev.Lett.* **102** (2009) 161802, [[arXiv:0809.4472](#)].
- [97] **CDF** Collaboration, T. Aaltonen *et. al.*, *Search for Long-Lived Massive Charged Particles in 1.96 TeV  $\bar{p}p$  Collisions*, *Phys.Rev.Lett.* **103** (2009) 021802, [[arXiv:0902.1266](#)].
- [98] G. Belanger, F. Boudjema, A. Pukhov, and A. Semenov, *micrOMEGAs: A program for calculating the relic density in the MSSM*, *Comput. Phys. Commun.* **149** (2002) 103–120, [[hep-ph/0112278](#)].
- [99] G. Belanger, F. Boudjema, P. Brun, A. Pukhov, S. Rosier-Lees, *et. al.*, *Indirect search for dark matter with micrOMEGAs2.4*, *Comput.Phys.Comm.* **182** (2011) 842–856, [[arXiv:1004.1092](#)].
- [100] T. Asaka, K. Hamaguchi, and K. Suzuki, *Cosmological gravitino problem in gauge mediated supersymmetry breaking models*, *Phys. Lett.* **B490** (2000) 136–146, [[hep-ph/0005136](#)].
- [101] M. Fujii, M. Ibe, and T. Yanagida, *Upper bound on gluino mass from thermal leptogenesis*, *Phys. Lett.* **B579** (2004) 6–12, [[hep-ph/0310142](#)].
- [102] C. F. Berger, L. Covi, S. Kraml, and F. Palorini, *The number density of a charged relic*, *JCAP* **0810** (2008) 005, [[arXiv:0807.0211](#)].
- [103] A. Freitas, F. D. Steffen, N. Tajuddin, and D. Wyler, *Late Energy Injection and Cosmological Constraints in Axino Dark Matter Scenarios*, *Phys. Lett.* **B682** (2009) 193–199, [[arXiv:0909.3293](#)].
- [104] J. Hasenkamp and J. Kersten, *Leptogenesis, Gravitino Dark Matter and Entropy Production*, *Phys.Rev.* **D82** (2010) 115029, [[arXiv:1008.1740](#)].
- [105] J. F. Gunion and H. E. Haber, *The CP conserving two Higgs doublet model: The Approach to the decoupling limit*, *Phys.Rev.* **D67** (2003) 075019, [[hep-ph/0207010](#)].
- [106] M. Endo, K. Hamaguchi, and K. Nakaji, *Probing High Reheating Temperature Scenarios at the LHC with Long-Lived Staus*, *JHEP* **1011** (2010) 004, [[arXiv:1008.2307](#)].
- [107] J. Hisano and S. Sugiyama, *Charge-breaking constraints on left-right mixing of stau’s*, *Phys.Lett.* **B696** (2011) 92–96, [[arXiv:1011.0260](#)].
- [108] A. D. Linde, *Decay of the False Vacuum at Finite Temperature*, *Nucl.Phys.* **B216** (1983) 421.
- [109] J. Espinosa, *Dominant two loop corrections to the MSSM finite temperature effective potential*, *Nucl.Phys.* **B475** (1996) 273–292, [[hep-ph/9604320](#)].
- [110] M. Endo, K. Hamaguchi, and K. Nakaji, *LHC signature with long-lived stau in high reheating temperature scenario*, [arXiv:1105.3823](#).
- [111] **Heavy Flavor Averaging Group** Collaboration, D. Asner *et. al.*, *Averages of b-hadron, c-hadron, and tau-lepton Properties*, [arXiv:1010.1589](#).
- [112] **ATLAS** Collaboration, Schumacher *et. al.*, *Higgs Boson Searches with ATLAS based on 2010 Data*, [arXiv:1106.2496](#).
- [113] **CMS** Collaboration, S. Chatrchyan *et. al.*, *Search for Neutral MSSM Higgs Bosons Decaying to Tau Pairs in pp Collisions at  $\sqrt{s} = 7$  TeV*, [arXiv:1104.1619](#).
- [114] T. Hahn, *Generating Feynman diagrams and amplitudes with FeynArts 3*, *Comput.Phys.Comm.* **140** (2001) 418–431, [[hep-ph/0012260](#)].

- [115] T. Hahn and M. Perez-Victoria, *Automatized one loop calculations in four-dimensions and D-dimensions*, *Comput.Phys.Commun.* **118** (1999) 153–165, [[hep-ph/9807565](#)].
- [116] M. Frank, T. Hahn, S. Heinemeyer, W. Hollik, H. Rzehak, *et. al.*, *The Higgs Boson Masses and Mixings of the Complex MSSM in the Feynman-Diagrammatic Approach*, *JHEP* **0702** (2007) 047, [[hep-ph/0611326](#)].
- [117] **LHC Higgs Cross Section Working Group** Collaboration, S. Dittmaier, C. Mariotti, G. Passarino, and R. E. Tanaka, *Handbook of LHC Higgs Cross Sections: 1. Inclusive Observables*, [arXiv:1101.0593](#).
- [118] L. J. Hall, R. Rattazzi, and U. Sarid, *The Top quark mass in supersymmetric SO(10) unification*, *Phys.Rev.* **D50** (1994) 7048–7065, [[hep-ph/9306309](#)].
- [119] R. Hempfling, *Yukawa coupling unification with supersymmetric threshold corrections*, *Phys.Rev.* **D49** (1994) 6168–6172.
- [120] M. S. Carena, M. Olechowski, S. Pokorski, and C. Wagner, *Electroweak Symmetry Breaking and Bottom-Top Yukawa Unification*, *Nucl.Phys.* **B426** (1994) 269–300, [[hep-ph/9402253](#)].
- [121] D. M. Pierce, J. A. Bagger, K. T. Matchev, and R.-j. Zhang, *Precision corrections in the minimal supersymmetric standard model*, *Nucl.Phys.* **B491** (1997) 3–67, [[hep-ph/9606211](#)].
- [122] M. S. Carena, D. Garcia, U. Nierste, and C. E. Wagner, *Effective Lagrangian for the  $t\bar{b}H^+$  interaction in the MSSM and charged Higgs phenomenology*, *Nucl.Phys.* **B577** (2000) 88–120, [[hep-ph/9912516](#)].
- [123] S. Heinemeyer, W. Hollik, H. Rzehak, and G. Weiglein, *High-Precision Predictions for the MSSM Higgs Sector at  $O(\alpha_b\alpha_s)$* , *Eur.Phys.J.* **C39** (2005) 465–481, [[hep-ph/0411114](#)].
- [124] A. Djouadi, *The Anatomy of electro-weak symmetry breaking. II. The Higgs bosons in the minimal supersymmetric model*, *Phys.Rept.* **459** (2008) 1–241, [[hep-ph/0503173](#)].
- [125] A. Martin, W. Stirling, R. Thorne, and G. Watt, *Parton distributions for the LHC*, *Eur.Phys.J.* **C63** (2009) 189–285, [[arXiv:0901.0002](#)].
- [126] A. R. Raklev, *Massive Metastable Charged (S)Particles at the LHC*, *Mod.Phys.Lett.* **A24** (2009) 1955–1969, [[arXiv:0908.0315](#)].
- [127] CMS-PAS-EXO-08-003, *Search for heavy stable charged particles with 100 inverse picobarns and 1 inverse femtobarn in the cms experiment*, [cdsweb.cern.ch/record/1152570?ln=en](#).
- [128] A. De Roeck, J. R. Ellis, F. Gianotti, F. Moortgat, K. Olive, *et. al.*, *Supersymmetric benchmarks with non-universal scalar masses or gravitino dark matter*, *Eur.Phys.J.* **C49** (2007) 1041–1066, [[hep-ph/0508198](#)].
- [129] **ATLAS** Collaboration, G. Aad *et. al.*, *Search for stable hadronising squarks and gluinos with the ATLAS experiment at the LHC*, [arXiv:1103.1984](#).
- [130] **CMS** Collaboration, V. Khachatryan *et. al.*, *Search for Heavy Stable Charged Particles in pp collisions at  $\sqrt{s} = 7$  TeV*, *JHEP* **1103** (2011) 024, [[arXiv:1101.1645](#)].
- [131] J. Heisig and J. Kersten, *Production of long-lived staus in the Drell-Yan process*, [arXiv:1106.0764](#).
- [132] W. Porod, *SPheno, a program for calculating supersymmetric spectra, SUSY particle decays and SUSY particle production at  $e^+e^-$  colliders*, *Comput.Phys.Commun.* **153** (2003) 275–315, [[hep-ph/0301101](#)].

- [133] A. Arbey and F. Mahmoudi, *SuperIso Relic v3.0: A program for calculating relic density and flavour physics observables: Extension to NMSSM*, *Comput.Phys.Commun.* **182** (2011) 1582–1583.
- [134] M. Drees and S. P. Martin, *Implications of SUSY model building*, **hep-ph/9504324**. Report of Subgroup 2 of the DPF Working Group on 'Electroweak Symmetry Breaking and Beyond the Standard Model'.
- [135] **CMS** Collaboration, G. Bayatian *et. al.*, *CMS technical design report, volume II: Physics performance*, *J.Phys.G* **G34** (2007) 995–1579.
- [136] **LHCb** Collaboration, R. Aaij *et. al.*, *Search for the rare decays  $B_s \rightarrow \mu\mu\mu$  and  $B_d \rightarrow \mu\mu\mu$* , *Phys.Lett.* **B699** (2011) 330–340, [[arXiv:1103.2465](#)].
- [137] H. E. Haber, *Higgs boson masses and couplings in the minimal supersymmetric model*, **hep-ph/9707213**. To appear in Perspectives on Higgs Physics II, Gordon L. Kane ed., World Scientific, Singapore, 1997.
- [138] J. Germer, W. Hollik, and E. Mirabella, *Hadronic production of bottom-squark pairs with electroweak contributions*, *JHEP* **05** (2011) 068, [[arXiv:1103.1258](#)].